

Interfacing Superconductor and Semiconductor Digital Electronics

Yerzhan Mustafa and Selçuk Köse

Abstract—Interface circuits are the key components that enable the hybrid integration of superconductor and semiconductor digital electronics. The design requirements of superconductor-semiconductor interface circuits vary depending on the application, such as high-performance classical computing, superconducting quantum computing, and digital signal processing. In this survey, various interface circuits are categorized based on the working principle and structure. The superconducting output drivers are explored, which are capable of converting and amplifying, *e.g.*, single flux quantum (SFQ) voltage pulses, to voltage levels that semiconductor circuits can process. Several trade-offs between circuit- and system-level design parameters are examined. Accordingly, parameters such as the data rate, output voltage, power dissipation, layout area, thermal/heat load of cryogenic cables, and bit-error rate are considered.

I. INTRODUCTION

Superconductor digital electronics such as single flux quantum (SFQ) logic is a promising candidate for beyond-CMOS (complementary metal–oxide–semiconductor) technology due to the high-speed operation of tens to hundreds of GHz and low energy consumption of 10^{-19} J per switching activity [1]–[5]. SFQ circuits comprise a wide variety of logic families such as rapid SFQ (RSFQ) [1], energy-efficient RSFQ (ERSFQ) [6], energy-efficient SFQ (eSFQ) [7], reciprocal quantum logic (RQL) [8], adiabatic quantum flux parametron (AQFP) [9], pulse conserving logic (PCL) [10], and superconducting sustainable ballistic fluxon (SSBF) [11]. All of these logic families use Josephson junctions (JJs) as a switching element and operate at cryogenic temperatures (*e.g.*, 4 K).

Despite delivering significant performance gains, superconductor digital electronics are not expected to fully replace advanced semiconductor (*e.g.*, CMOS) technology. A hybrid approach, which leverages the key advantages of both superconductor and semiconductor technologies, is beneficial. Early applications of superconductor digital electronics include microprocessors [12]–[17], accelerators [18], [19], digital radio frequency (RF) receivers [20]–[23], and control and readout circuits for superconducting quantum computers [24]–[34]. Semiconductor electronics is typically used to complement certain limitations of superconductor circuits such as low-density memory [35]–[39].

The hybrid integration of superconductor and semiconductor electronics requires special interface circuits to convert

Y. Mustafa and S. Köse are with the Department of Electrical and Computer Engineering, University of Rochester, Rochester, NY, 14627, USA. E-mails: (yerzhan.mustafa@rochester.edu, selcuk.kose@rochester.edu).

This work is supported in part by the National Science Foundation Expeditions Award under Grant CCF-2124453 and SHF Award under Grant CCF-2308863, and Department of Energy EXPRESS program under Grant DE-SC0024198.

signaling between two different technologies. Semiconductor circuits (*e.g.*, CMOS) encode logical ‘1’ and ‘0’ into constant (DC) high and low voltage levels, respectively, in the order of hundreds of mV to a few volts, depending on the fabrication node. Superconductor circuits such as SFQ logic encode logical ‘1’ and ‘0’ into the presence and absence of voltage pulses, respectively. These voltage pulses are typically about 1 mV in amplitude and approximately 2 ps in duration and have a constant value equal to one magnetic flux quantum when integrated over time ($\Phi_0 \approx 2.07 \times 10^{-15}$ Wb) [1]. A particular challenge is to convert and amplify SFQ pulses to appropriate voltage signals that CMOS circuits can process. The low driving capability of JJs introduces certain trade-offs in amplification gain, power dissipation, layout area, and other parameters of superconductor-semiconductor interface circuits.

In this paper, various interface circuits, which are used between superconductor and semiconductor digital electronics, are explored. First, existing applications of superconductor digital electronics are discussed, and the need for interface circuits is detailed in Section II. A taxonomy of superconductor-semiconductor interface circuits is presented in Section III with a detailed discussion of the working principle and structure of each circuit type. The implications of different fabrication technologies on the performance of interface circuits are analyzed in Section IV. A comparison of superconducting output drivers, a subset of superconductor-semiconductor interface circuits, is provided based on circuit- and system-level criteria in Section V. The conclusions are drawn in Section VI.

II. THE NEED FOR SUPERCONDUCTOR-SEMICONDUCTOR INTERFACE CIRCUITS

The superconductor-semiconductor interface circuits are essential building blocks in establishing communication between various cryogenic (superconducting) technologies and the room-temperature electronics. The following is a list of emerging applications that utilize superconductor digital electronics and require a specialized interface to semiconductor circuits.

High-performance computing (HPC): Superconductor digital electronics (*e.g.*, SFQ logic) can operate at extremely high switching frequency of tens to hundreds of GHz while consuming 10^{-19} J energy per switching activity [1]–[5]. These characteristics make this technology a promising candidate for beyond-CMOS technology, particularly, for HPC such as data centers and cloud computing [2]–[5]. Several 8-bit microprocessors have been designed using SFQ logic [12],

[13], [15]–[17]. For example, the microprocessor in [16] is capable of operating at 57.2 GHz with a power consumption of 11.2 mW. An SFQ-based microprocessor needs a cryogenic memory to store and load various instructions and data. Various types of cryogenic memory are available in the literature, as reviewed in [40]. A hybrid approach, which uses semiconductor-based (*e.g.*, CMOS) memory, offers high storage capacity/density and fabrication maturity as compared to other cryogenic memories [40]. This type of memory is known as Josephson-CMOS hybrid memory [37]–[39]. Therefore, interface circuits are needed to convert signals between superconducting microprocessor and semiconductor memory. A recent spin-out of IMEC, Snowcap Compute, Inc., is working on building artificial intelligence computing chips using superconductor digital electronics [18], [41].

Quantum computing: To realize a quantum computer that can compete with modern CMOS based computing devices, a large number of qubits are needed. One promising approach to scaling superconducting quantum computers is placing the qubit control and readout circuitry in close proximity to the qubits (*i.e.*, within the same temperature zone) to reduce the thermal load from cryogenic interconnects. SFQ technology is an emerging approach to the control and readout of superconducting qubits because of its ultra-low-power dissipation [24]–[30]. Companies such as SEEQC and Atlantic Quantum (recently acquired by Google Quantum AI [42]) are working on developing quantum computers with superconductor digital circuits to enable large-scale control and readout [31]–[34], [43].

Qubits are prone to errors (decoherence) due to sensitivity to the environment. To overcome this challenge, quantum error correction (QEC) is needed. Fast, real-time correction of qubits can be achieved using graphics processing units (GPUs) due to their highly parallelizable processing capabilities. GPUs, which are made with semiconductor technology, can accelerate the decoding of error syndromes and determine the required corrections. High-speed superconductor-semiconductor interface circuits can therefore facilitate fast QEC. For example, SEEQC in collaboration with NVIDIA develops the first fully digital quantum-classical interface for ultra-low latency QEC [44], [45].

Digital signal processing: A software-defined radio is a communication system in which instead of analog hardware, broadband RF signals are converted into digital form [46]. Due to the high frequency operation of SFQ logic (*i.e.*, tens of GHz), superconductor digital RF receivers are capable of direct digitization of RF signals in the range of kHz to GHz [20]–[23]. For example, HYPRES, Inc. offers a commercially available digital RF receiver [47]. This system uses 17-channel interface amplifiers, which enable communication between superconductor (*i.e.*, SFQ) and semiconductor (*i.e.*, field-programmable gate array (FPGA)) circuits [47].

Single-photon detectors: Superconducting single-photon detectors include superconductor nanostrip photon detector (SNSPD) [48], [49] and transition edge sensor (TES) [50]–[52]. Note that SNSPD nomenclature is based on International Electrotechnical Commission standard, which redefines commonly used ‘superconducting nanowire single-photon detec-

tor’ term [53]. These detectors can provide higher detection efficiency, lower dark counts, and faster response times as compared to semiconductor-based detectors [49], [51], [52]. Nevertheless, single-photon detectors should operate at cryogenic temperatures and, hence, require an interface circuitry to send the data to room-temperature electronics. For example, superconductor electronic circuits are used to readout SNSPD [54]–[60] and TES [61]–[66].

Neuromorphic computing: Superconductor electronics can be used to implement neuromorphic computing systems at the hardware-level. JJs are basic building blocks of superconductor electronic circuits [1]. The spiking nature of brain neurons could be mimicked with JJs, which produce voltage pulses during switching [67]. Moreover, a near lossless transmission of these voltage pulses over superconducting transmission lines enables fast and energy-efficient operation of neuromorphic circuits [67]. Neuromorphic computing hardware types that are implemented with superconductor electronic circuits and devices have been reviewed in [67], [68]. Neuromorphic computing requires memory elements to store synapse weights [67]. While novel superconductor-based memory is an ongoing research, the hybrid approach that uses mature, high-capacity semiconductor memory is preferred similar to HPC systems [40]. Additionally, superconductor-semiconductor interface circuits are essential components for testing the performance of novel superconducting neuromorphic circuits and architectures as, *e.g.*, implemented in [69], [70].

The aforementioned applications use superconductor-semiconductor interface circuits under various design requirements and limitations such as data rate, gain (amplification), operating temperature (*e.g.*, 20 mK, 4 K, 50 K, etc.), power dissipation, and fabrication technology. As a result, various types of interface circuits with different characteristics have been proposed in the literature. Therefore, it is important to categorize and identify the unique advantages and drawbacks of each type of interface circuit.

III. TAXONOMY OF SUPERCONDUCTOR-SEMICONDUCTOR INTERFACE CIRCUITS

Digital data links with superconductor-semiconductor interface circuits typically consist of two stages. The first stage is a superconducting output driver that receives a signal from superconductor digital electronics (*e.g.*, SFQ pulse), converts, and amplifies it to a DC signal in the range of hundreds of μ V to hundreds of mV. The second stage is a semiconductor amplifier that further boosts the DC signal up to the level of CMOS technology (around 1 V) [71]. Alternatively, a photonic circuit can be used as the second stage such as an electro-optic modulator (EOM) [72]–[78] or vertical cavity surface emitting lasers (VCSEL) [79]–[83]. A block diagram of the cryostat housing superconductor, semiconductor, photonic, and quantum chips is depicted in Fig. 1(a). The key components of the superconductor-semiconductor interface are highlighted in green in Fig. 1(a). It should be noted that the input drivers (see Fig. 1(a)) are also part of the superconductor-semiconductor interface circuits. Due to the straightforward nature of converting DC voltage signals from semiconductor

circuits to SFQ pulses, input-side interfaces such as DC-to-SFQ converters [84]–[87] are commonly reused across many designs. In contrast, the output stage presents substantially greater design difficulty and admits a wider range of circuit implementations. Therefore, the focus of this work is placed on the output drivers.

A taxonomy of superconducting output drivers is shown in Fig. 1(b). In this classification, output drivers are grouped into two major categories: 1) JJ-based and 2) multi-terminal devices.

A. JJ-based output drivers

JJ-based output drivers use JJs as a switching element. A JJ is a two-terminal device that consists of two superconductor materials separated by a weak link (e.g., Nb/AlO_x/Nb). JJs are commonly used in SFQ logic and superconducting quantum circuits, and have multiple established fabrication processes (e.g., MIT Lincoln Lab SFQ5ee [88], SEEQC SFQ-C5SL [89], ADP2 [90], SIMIT Nb03P [91], and FLUXONICS CJ2 [92]). Depending on the type of JJ damping, JJ-based output drivers can be grouped into two classes, as depicted in (Fig. 1(b)). The first class consists of latching drivers, which employ underdamped junctions characterized by a Stewart-McCumber parameter $\beta_c > 1$ [4]. The second class consists of SQUID (superconducting quantum interference device)-based drivers, which rely on overdamped or critically damped junctions, respectively, with $\beta_c < 1$ and $\beta_c = 1$.

1) **Latching drivers:** In latching drivers, the underdamped JJs exhibit hysteretic behavior. Once the current flowing through these types of JJs exceeds the critical value, the junction switches from superconducting state to resistive state. The JJ is latched in the resistive state until its current is reduced below a specific threshold value (known as return current). The following are examples of latching driver circuits.

Four-junction logic (4JL) gate: A 4JL gate was initially proposed in 1980 by Takada *et al.* [93], [94] as a logic gate (AND, OR, and NOT) for superconducting latching logic. While latching logic was largely displaced by SFQ technology in the early 1990s due to the higher available clock rates [3], the 4JL gate circuit remains a practical and effective option for use as a superconducting output driver. The schematic of a 4JL gate is depicted in Fig. 2(f), which consists of five underdamped JJs, where four JJs come from the original logic circuit [93] and one JJ is used as a buffer to prevent a back-action to the SFQ input circuits. The critical current of these JJs is chosen such that $I_{c1} = I_{c2} = I_{c,in} = 100 \mu\text{A}$ and $I_{c3} = I_{c4} = 300 \mu\text{A}$ [37], [95], [96]. The operating principle of the 4JL gate is illustrated through simulations in Fig. 3(f). All JJs are initially biased at approximately 80% of their critical currents, and an SFQ pulse is applied at the input terminal V_{in} . This SFQ pulse first switches the bottom left JJ with critical current I_{c1} from the superconducting state to the resistive state. The resulting imbalance in the bias (supply) current distribution directs most of the bias current into the JJs on the right branch (with I_{c3} and I_{c4}), effectively switching them to the resistive state. Finally, the top left JJ (with I_{c2}) and the buffer JJ (with $I_{c,in}$) transition to the resistive state.

Once all JJs switch to the resistive state, the circuit produces an output voltage approximately twice the gap voltage $2V_g$. In Fig. 3(f), an output voltage of about 5 mV is produced for MIT Lincoln Lab SFQ5ee process [88] with $V_g = 2.8 \text{ mV}$. To restore the 4JL gate to the superconducting state, the bias voltage V_b is turned off once per clock cycle, generating a square-wave (AC) waveform, as shown in Fig. 3(f).

The 4JL gate is commonly used in 4 K Josephson-CMOS hybrid memories as a pre-amplifier for Suzuki stack circuit [37]–[39], [96]. Additionally, 4JL gate can be used as an output driver for digital data links from 4 K to 50 K temperature zones [105].

Suzuki stack: A Suzuki stack (a.k.a. Josephson latching driver) was first proposed in 1988 by Suzuki *et al.* [106]. A schematic of a Suzuki stack circuit is depicted in Fig. 2(d). The Suzuki stack consists of two arrays of serially connected underdamped JJs. Each branch has a small resistor R_{br} (around 3-4 Ω) to avoid flux quantization [99]. In a conventional design, all JJs have an equal critical current (e.g., 400 μA) [37], [96], [99]. For an n number of JJs in series, the Suzuki stack can produce an output voltage of nV_g . Depending on the application, typical values of n are in the range of 4 to 24 [37], [38], [92], [96], [99], [106]–[128]. The operating principle of a 16-JJ (*i.e.*, $n = 16$) Suzuki stack circuit is shown in Fig. 3(e). The input signal is a 140 μA current pulse, which models the signal sent from the 4JL gate pre-amplifier [99]. Although a Suzuki stack can be driven with an SFQ pulse as was demonstrated in [92], [109], [113], [116], [118], a 4JL gate pre-amplifier offers improved input and output stability [37]. Additionally, the lowermost left JJ (with I_{c1}) in the Suzuki stack can be replaced with two JJs in series [37], [96], [108], 2-JJ (or 3-JJ) SQUID structure [116], [125] for higher input sensitivity and wider bias margins.

With MIT Lincoln Lab SFQ5ee process, the 16-stage Suzuki stack can produce an output voltage of around 45 mV as shown in Fig. 3(e). The switching mechanism of the Suzuki stack is similar to that of the 4JL gate [121].

Both 4JL gate and Suzuki stack typically require an AC bias voltage, which introduces several challenges including synchronization issues, coupling effects, and increased heat load of cryogenic bias cables [37], [129], [130]. The coupling effects can be mitigated by adding a top niobium (Nb) layer over the SFQ circuits, which acts as a magnetic shield [37]. Alternatively, DC-biased Suzuki stack designs have been proposed to address these drawbacks in [129], [131], [132].

In a multi-channel setup with a single power supply, Suzuki stacks require a large bias resistor R_b (Fig. 2(d)), typically around 750 Ω [37], [99]. Consequently, most of the power is dissipated across R_b [99]. To address this, a power optimization technique is proposed in [120], which employs unequal critical current values for the JJs in the left and right branches. This approach effectively reduces power dissipation by 30–70%.

As noted earlier, Suzuki stack circuits (with 4JL gate pre-amplifiers) are widely used in 4 K Josephson-CMOS hybrid memories [37]–[39]. Among the various JJ-based output drivers, a Suzuki stack is capable of producing the highest output voltages, typically ranging from tens to hundreds of

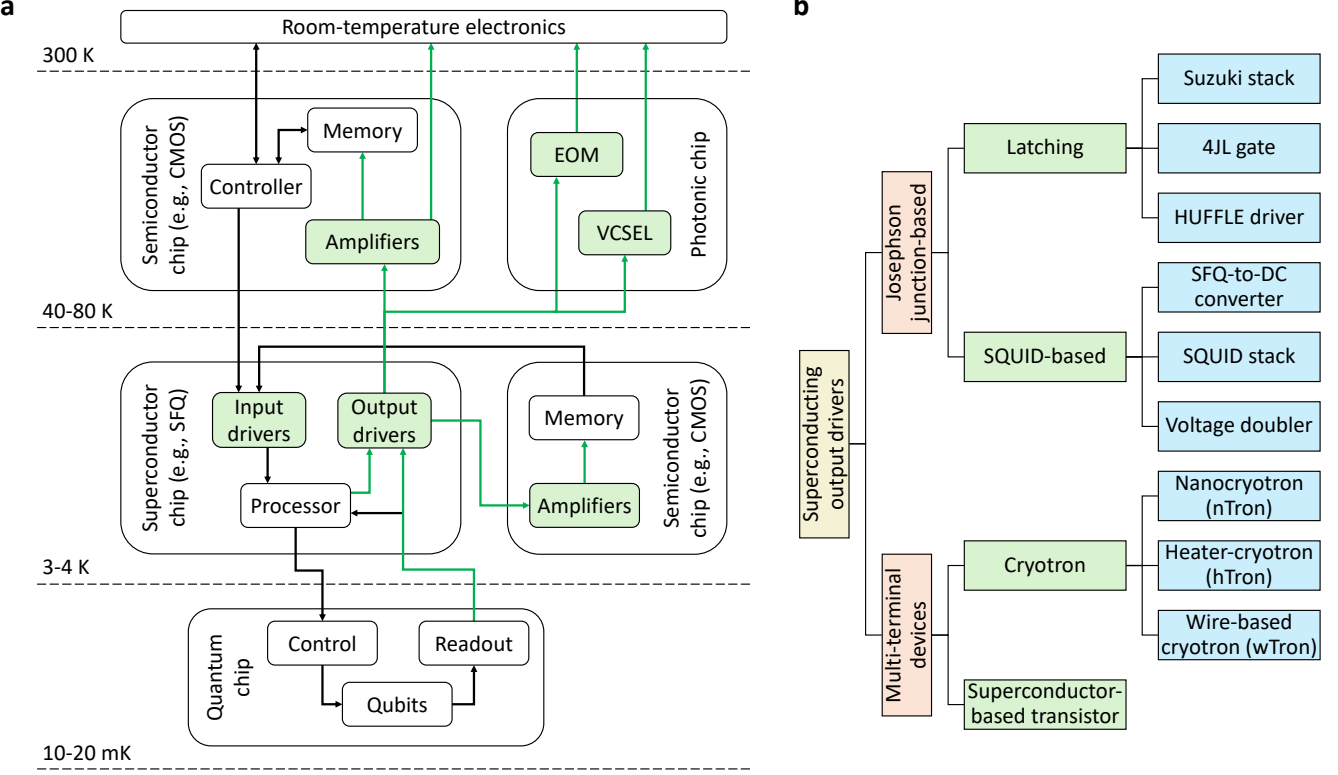


Fig. 1. **a**, Block diagram of the cryostat with superconductor, semiconductor, photonic, and quantum chips. The superconductor-semiconductor interface circuits are highlighted in green boxes. Digital output data links are shown with green arrows. **b**, Taxonomy of the superconducting output drivers.

millivolts [38], [96], [99], [106], [108], [121]. A higher output voltage of Suzuki stack circuit is particularly necessary in 4 K to 4 K digital data links (*e.g.*, sending the data from an SFQ chip to 4 K memory as shown in Fig. 1(a)). As a result, a subsequent semiconductor amplifier stage would require a lower gain and, hence, dissipate less power, which benefits the overall cooling power budget at 4 K. Although the operating frequency of Suzuki stack circuits is limited to a few GHz due to the latching-type of switching, this frequency is sufficient for direct interfacing with CMOS memory. For example, a 4 K Josephson-CMOS memory operating at 1 GHz is demonstrated in [38].

Hybrid unlatching flip-flop logic element (HUFFLE) driver: The HUFFLE circuit was introduced in 1979 by Hebard *et al.* [98] as a DC-biased flip-flop logic element for latching logic. The schematic of a HUFFLE circuit is depicted in Fig. 2(b). The circuit comprises two gates G_1 and G_2 , which can be, for example, individual underdamped JJs or interferometers [98], along with an output inductor L_{out} and two resistors, R_1 and R_2 . The circuit includes two DC bias lines and two control currents (I_{con1} and I_{con2}), as illustrated in Fig. 2(b). The operating principle of the HUFFLE circuit is shown in Fig. 3(d). G_1 and G_2 are used as individual JJs coupled to inductive lines with I_{con1} and I_{con2} , respectively. Initially, both G_1 and G_2 are in the superconducting state, allowing bias current to flow through them. When I_{con1} is applied, G_1 switches to the resistive state, diverting the bias

current through R_1 , L_{out} , and G_2 . Although the current in G_1 remains above the return current, G_1 stays in the resistive state. Upon application of I_{con2} , G_2 switches to the resistive state, momentarily reducing the bias current through G_1 and causing it to return to the superconducting state. After that, the bias current flows through R_2 , L_{out} , and G_1 .

The HUFFLE circuit has been demonstrated in a ring oscillator in [133] producing roughly 2 mV at 0.5 GHz frequency. A comprehensive theoretical analysis of the HUFFLE circuit is presented in [134]. The HUFFLE circuit has been used as an output driver in [135], [136]. In [135], G is a 3-JJ interferometer, which is controlled by the SFQ-to-DC converter. This driver was able to produce roughly 1.5 mV with an estimated frequency of 4 GHz. In [136], G is an SFQ-to-DC converter with unshunted (*i.e.*, underdamped) JJs. This driver produced an output voltage of 2.8 mV [136]. While the HUFFLE driver offers a DC-biased design without coupling and synchronization issues, it is prone to a parasitic ‘hang-up’ (‘latch-up’) mode, where both G_1 and G_2 latch to the voltage state, resulting in incorrect operation [134]. Therefore, this type of driver has not been commonly used in modern superconductor-based applications.

2) SQUID-based drivers: SQUID-based drivers use a DC SQUID structure [137], which consists of two overdamped (or critically damped) JJs in parallel, forming a superconducting loop, as shown in Fig. 2(a). A DC SQUID produces a periodic voltage response due to an external magnetic field [137]. Its period is equal to a magnetic flux quantum (Φ_0), and the

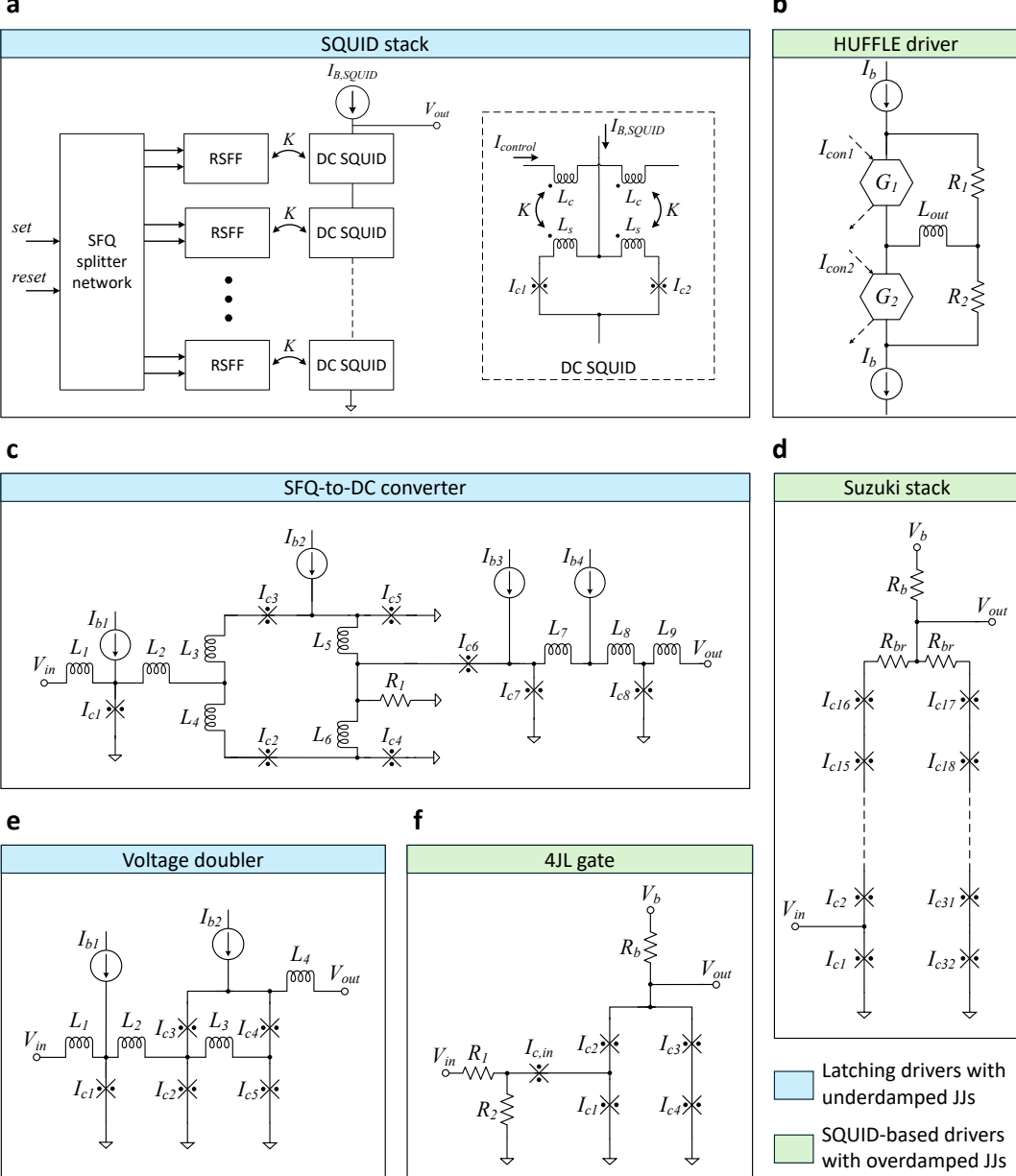


Fig. 2. Schematics of JJ-based output drivers. **a**, SQUID stack with RSFFs [97]. The inset shows the schematic of DC SQUID cell. **b**, HUFFLE driver [98]. **c**, SFQ-to-DC converter based on TFF [1], [86]. **d**, Suzuki stack with 16-JJ configuration [99]. **e**, Voltage doubler [100]. **f**, 4JL gate [37]. Shunt resistors and parasitic inductances of JJs are not shown. A novel symbol of JJ is used that is standardized by International Electrotechnical Commission [101].

maximum output voltage is achieved at the integer multiples of $\Phi_0/2$. SQUID-based drivers leverage this effect by digitally switching the DC SQUID(s) between zero applied flux and $\Phi_0/2$ flux. The following are examples of SQUID-based output driver circuits.

SQUID stack: A SQUID stack consists of multiple DC SQUIDs that are connected in series, as shown in Fig. 2(a). The first demonstration of a SQUID stack structure was made in 1991 by Welty *et al.* [138], where 100 DC SQUIDs were fabricated using trilayer Nb/AIO_x/Nb JJs. In a series connection, a DC SQUID can produce a higher output voltage by constructively interfering the switching from each DC SQUID. In a SQUID stack, each DC SQUID cell is magnetically

coupled to a line with the control current $I_{control}$. To produce the maximum output voltage, $I_{control}$ should be set such that $L_m I_{control} = \Phi_0/2$ [139]. L_m is the mutual inductance that can be expressed as $L_m = 2K\sqrt{L_c L_s}$, where L_c and L_s are the inductances, and K is the coupling coefficient, as shown in Fig. 2(a).

Several SFQ circuits have been proposed in the literature to generate the required $I_{control}$. For example, Fig. 2(a) illustrates a reset-set flip-flop (RSFF)-based approach in which the storage loop of the RSFF is magnetically coupled to the DC SQUID cell. The RSFF-based SQUID stack designs have been reported in [97], [103], [140]–[145]. The operating principle of a 16-stage SQUID stack employing RSFFs is illustrated in

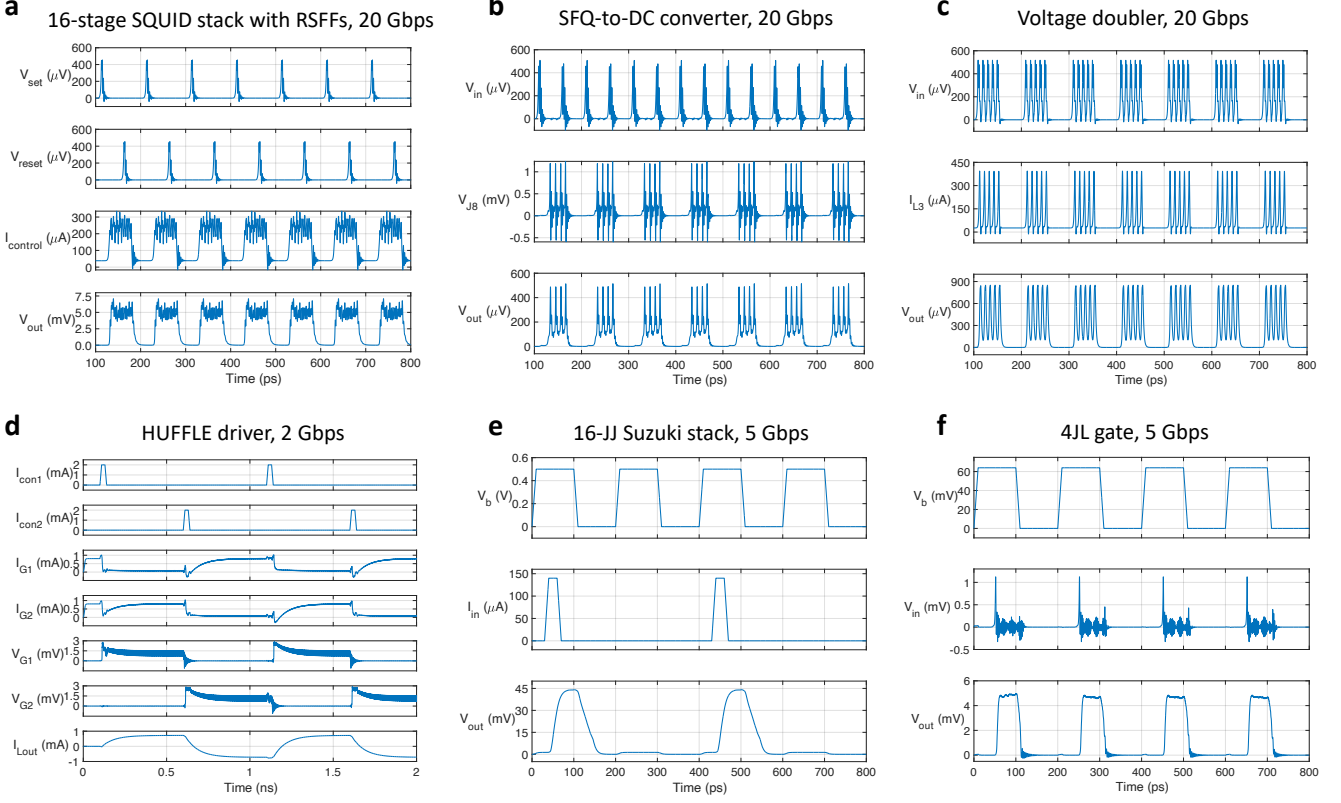


Fig. 3. Simulation of JJ-based output drivers. Simulated in JoSIM [102] using MIT Lincoln Lab SFQ5ee process with the critical current density of $100 \mu\text{A}/\mu\text{m}^2$ [88]. **a**, 16-stage SQUID stack with RSFFs, **b**, SFQ-to-DC converter, and **c**, voltage doubler are operating at 20 Gbps with 50Ω and 100 pH load. The input signal of voltage doubler is modeled as a 100 GHz SFQ pulse train [100]. **d**, HUFFLE driver operating at 2 Gbps with $L_{out} = 100 \text{ pH}$. **e**, 16-JJ Suzuki stack is operating at 5 Gbps with 50Ω , 100 pH , and 180 fF load. **f**, 4JL gate circuit is operating at 5 Gbps with 50Ω and 100 pH load. The circuit parameters are similar to designs presented in [37], [86], [98], [99], [103], [104].

Fig. 3(a). A *set* signal introduces a fluxon into the storage loop of the RSFFs, thereby increasing $I_{control}$ and producing an output voltage V_{out} of roughly 5 mV. Conversely, a *reset* signal removes the stored flux and turns off $I_{control}$. A non-return-to-zero (NRZ) signaling scheme can be implemented by driving the *set* and *reset* inputs with a toggle flip-flop (TFF) [97].

In addition to RSFF, SQUID stacks can also be driven using a Josephson transmission line (JTL) [139], [146], an SFQ-to-DC converter [147], [148], or a combination of both approaches [149]–[152]. SQUID stack circuits implemented using the RSFQ logic style [1] typically dissipate on the order of 100–200 μW [22], [145], [153], which is comparable to the power dissipation of Suzuki stacks [37], [38], [96], [99], [108], [121], [132], [154], [155]. Its power dissipation can be further reduced by employing energy-efficient logic families such as ERSFQ [6], eSFQ [7], and RQL [8]. For example, an RQL-based 32-stage SQUID stack has been demonstrated in [156], exhibiting a power dissipation of 320 nW.

In a symmetric DC SQUID cell, both JJs are shunted with identical resistors and share the same β_c parameter. An asymmetrical DC SQUID, where one of the JJs is unshunted and the other one is overdamped, can achieve a larger output voltage response as compared to a symmetrical design. SQUID stacks with asymmetrical DC SQUIDs have been presented

in [139], [144], [145], [157]. A double-SQUID design has been proposed in [158], where two DC SQUIDs share a common sensing inductor, achieving a two-fold increase in the output voltage. SQUID stacks with double-SQUIDs have been proposed in [159], [160]. A 4-JJ SQUID circuit housing two independent input transformers has been presented in [156], leveraging a unique switching mechanism inherent to AC-biased RQL logic. A SQIF (superconducting quantum interference filter)-based driver has been presented in [161] where each DC SQUID stage has a different loop size for broad band applications.

One of the challenges in designing SQUID stack circuits is that increasing the number of DC SQUIDs connected in series does not lead to a linear increase in the output voltage. To overcome such saturation and further increase the output voltage, SQUID stacks circuit can be connected in parallel, as suggested in [150]. Nevertheless, such a design requires additional control circuitry and results in a significantly larger layout area. To ensure the highest output voltage, the SQUID stacks require a careful (symmetric) layout design. Ideally, the control signals for each DC SQUID in the array should be synchronized and applied simultaneously to achieve constructive interference. To achieve this, an H-tree structure was proposed in [151] to equalize the propagation delay of the control signals.

State-of-the-art SQUID stack output drivers are capable of producing an output voltages of at least 5 mV at data rates of 20-30 Gbps [71], [103], [144], [145]. With these capabilities, SQUID stacks are commonly employed in digital data links operating from 4 K to higher temperature stages to drive both semiconductor amplifiers [71] and photonic circuits (*e.g.*, electro-optical modulators) [76]–[78]. Additionally, SQUID stack structures are commonly used in superconducting digital-to-analog (D/A) converters as a voltage multiplier circuit [153], [162], [163].

SFQ-to-DC converter: An SFQ-to-DC converter was presented in 1989 by Kaplunenko *et al.* [84]. The schematic of an SFQ-to-DC converter circuit is depicted in Fig. 2(c). The circuit consists of a single DC SQUID directly connected to the quantizing inductance of a TFF [1], [84]. Unlike in SQUID stack, the DC SQUID in this circuit has no magnetic coupling. The switching of the TFF induces a π -phase shift across the two JJs with I_{c4} and I_{c5} (Fig. 2(c)) effectively modulating the critical current of the SQUID [84]. The operating principle of an SFQ-to-DC converter is illustrated in Fig. 3(b). Each input SFQ pulse toggles the output voltage V_{out} between high and low states, implementing an NRZ signaling scheme.

Among JJ-based output drivers, an SFQ-to-DC converter provides the lowest power dissipation and highest data rates. However, it produces the lowest output voltage. For example, the SFQ-to-DC converter presented in [71] can produce a 1.3 mV signal at 40 Gbps while dissipating 13.4 μ W. Additionally, its power dissipation can be reduced down to 1.3 μ W using ERSFQ logic [71]. This output driver is included in the standard cell library of various SFQ logic families [85], [86], [164]–[166] and is typically available in the process design kit (PDK). Similar to SQUID stacks, SFQ-to-DC converters are commonly used in digital data links operating from 4 K to higher temperature stages [71], [79], [167]. Due to the lower output voltage as compared to SQUID stack, an SFQ-to-DC converter requires a more complex setup for semiconductor amplifiers [71] or a more sensitive photonic circuit (*e.g.*, VCSEL) [79]. Additionally, SFQ-to-DC converter structures can also be utilized as precise current generators to manipulate and bias superconducting qubits [28].

Voltage doubler: A voltage doubler (*a.k.a.* quasi-digital voltage amplifier (QDVA)) was presented in 1991 by Kaplunenko *et al.* in [104]. This voltage doubler consists of two DC SQUIDs that are strongly coupled via an inductance L_3 as depicted in Fig. 2(e). When an SFQ pulse is applied at the input terminal V_{in} , a flux quantum and anti-flux quantum pass through the bottom and top SQUIDs producing two SFQ pulses, which appear at the output terminal V_{out} [104]. The operating principle of the voltage doubler is illustrated in Fig. 3(c). A train of SFQ pulses with 100 GHz frequency is periodically applied. The average V_{out} generated is approximately two times larger than the average V_{in} .

The voltage doubler output driver can be used with an SFQ-to-DC converter as suggested in [100], [168]. In this configuration, the output voltage of an SFQ-to-DC converter is doubled with a voltage doubler (*e.g.*, from 200 μ V from SFQ-to-DC converter is increased to 438 μ V with the voltage doubler [100]). By repeating the voltage doubler structure in

vertical and horizontal directions, a larger factor of voltage multiplication can be achieved as proposed in [169]. In [169], a six-stage parallel QDVA is demonstrated to achieve a five-fold multiplication of the input signal amplitude.

A similar concept of doubling the output voltage was introduced in [170], where an SFQ pulse is converted into a double flux quantum (DFQ) pulse. By stacking several DFQ drivers in series, an output voltage of 1.30 mV can be produced at an estimated data rate of 10 Gbps [170]. To generate an SFQ pulse train, a voltage-controlled oscillator (VCO) and a non-destructive readout (NDRO) circuit are employed in [170]. In addition to the digital data transmission, stacked DFQ-based drivers are used in D/A converters for metrological applications. For example, a 20-fold DFQ amplifier has achieved a maximum output voltage of 2.90 mV [171]. A 1000-fold DFQ amplifier that achieves an output voltage of 43 mV has been presented in [172].

B. Multi-terminal devices

Superconducting multi-terminal devices have three or more terminals that resemble a semiconductor transistor. Multi-terminal devices suitable for use as output drivers can be classified into two main categories: cryotrons and superconductor-based transistors (Fig. 1(b)).

1) **Cryotron:** Cryotrons [173] consist of a superconducting channel through which current flows between the drain and source terminals, and an input terminal that receives the control signal to modulate the channel characteristics (*i.e.*, switching it to the resistive state). The following subsections describe several variations of cryotron-based output drivers.

Nanocryotron (nTron): nTron was proposed in 2014 by McCaughan and Berggren [174]. The layout view and circuit symbol of nTron are depicted in Fig. 4(a) and Fig. 4(e), respectively. An nTron is implemented with a single superconductor layer (*e.g.*, NbN [174], [175] or NbTiN [176], [177]) that is shaped in a specific way, as shown in Fig. 4(a). Particularly, the nTron has an input gate that injects a small amount of current, creating a localized, Joule-heat hotspot in the choke area (Fig. 4(a)). As a result of the rapid transition from the superconducting to the resistive state, an nTron can drive large impedance loads (more than 100 k Ω) [174].

An nTron can be triggered with SNSPD pulses [174]. Additionally, it can interface directly with SFQ circuits, as experimentally demonstrated in [175], enabling seamless integration without the need for intermediate signal conditioning stages. As compared to JJ-based output drivers, an nTron offers the largest output voltage ranging from 100 mV up to 8.1 V [174], [176], [177]), while simultaneously achieving quite low power dissipation (around 8 nW [175]), and extremely compact layout footprint of roughly 0.1 μ m², excluding the bias inductors [175]. However, the primary limitation is the low switching frequency of around 1 GHz, which arises from the relatively long transition times required for the device to switch between superconducting and resistive states [175]. Additionally, an nTron can be configured to operate in either self-reset or latched modes and can therefore be biased using a DC or AC power supply, respectively [175].

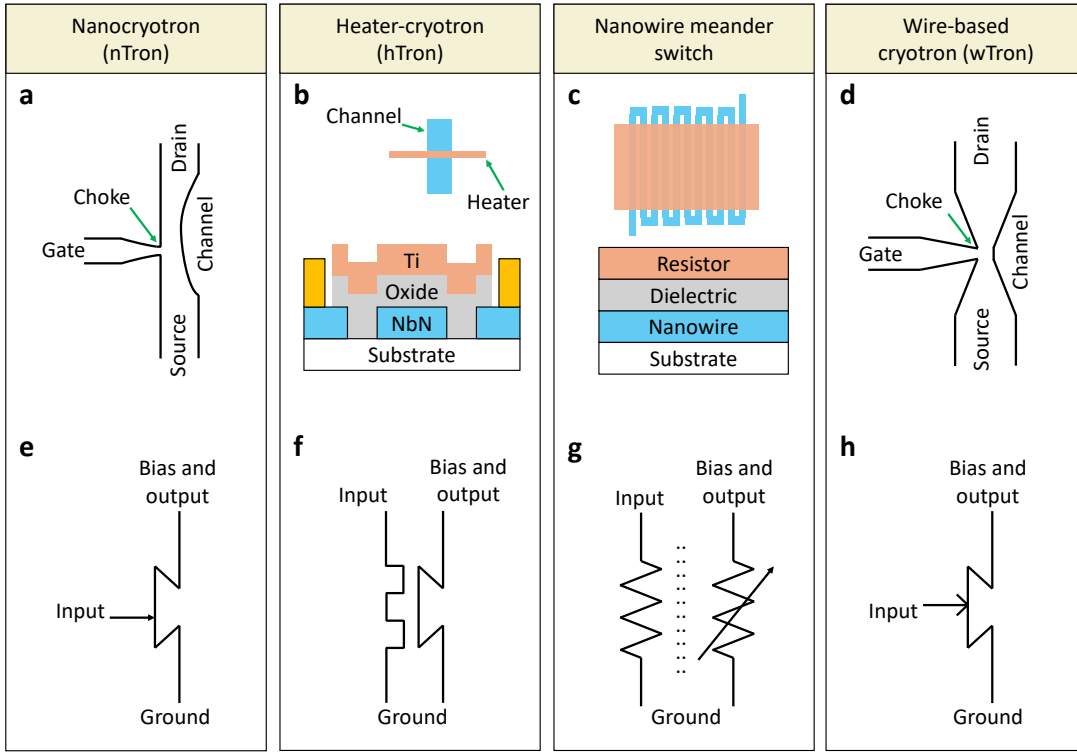


Fig. 4. Multi-terminal devices. Layout view/structure of **a**, nanocryotron (nTron) [174], **b**, multi-layered heater-cryotron (hTron) [178], **c**, nanowire meander switch [179], and **d**, wire-based cryotron (wTron) [180]. The circuit symbols of **e**, nTron, **f**, multi-layered hTron, **g**, nanowire meander switch, and **h**, wTron.

The nTron fabrication process is based on SNSPD technology [180]. Therefore, nTrons can be integrated on the same chip with SNSPDs and employed for their readout [59], [60]. In the case of interfacing SFQ circuits, nTrons typically need to be fabricated on a separate chip and then, for example, wire bonded to the SFQ and CMOS chips [175]–[177]. An nTron can also serve as an output driver for 4 K Josephson-CMOS hybrid memory, as suggested in [176]. It is estimated that a Josephson-CMOS hybrid memory incorporating nTrons could achieve roughly 1/12 of the power dissipation of conventional Suzuki stack-based hybrid memory architectures [176]. Nevertheless, nTron fabrication techniques require further development along with more advanced circuit-level simulation models [177], [181].

Heater-cryotron (hTron): An hTron was presented in 2018 by Zhao *et al.* [182]. The first version of the hTron had a planar structure with two isolated and closely spaced (40 nm spacing) nanowires [182]. A multi-layered hTron was presented later in [178]. The physical layout and circuit symbol of a multi-layered hTron are depicted in Fig. 4(b) and Fig. 4(f), respectively. The device consists of channel and heater nanowires, making it a four-terminal device. Due to the electrical isolation of the heater (*i.e.*, input) and the channel, an hTron does not experience a current leakage problem, unlike an nTron [178]. When an input signal is applied to the heater, it transitions from the superconducting state to the resistive state. Due to the local temperature increase caused by Joule heating and the close proximity of the heater, the channel's critical current is suppressed, causing it to switch to the resistive state.

hTrons have been employed in the design of superconducting memory elements [182], [183], cryogenic logic cells [184], and SNSPD readout circuits [178]. Similar to nTrons, hTrons are capable of producing large output voltages on the order of 500–600 mV [178], [183]. A SPICE model for the hTron device is proposed in [185].

Nanowire meander switch: A nanowire meander switch has been proposed in [179]. This device has a similar structure and switching mechanism as an hTron, as illustrated in Fig. 4(c) with the corresponding circuit symbol depicted in Fig. 4(g). In this four-terminal device, the channel is a nanowire meander and the heater is a wide resistor line. The nanowire meander switch can deliver a 1.12 V output voltage, which is sufficient to drive a cryogenic light-emitting diode (LED), as demonstrated in [179]. The switch exhibits a turn-on time of less than 300 ps and a turn-off time of approximately 15 ns. This relatively long thermal recovery time of the switch can be advantageous in optoelectronic applications (*e.g.*, driving LEDs and modulators) and neuromorphic circuits [186].

Wire-based cryotron (wTron): A wTron was presented in 2025 by Paul *et al.* [180]. This device has a similar structure and switching mechanism as nTron, as illustrated in Fig. 4(d). The corresponding circuit symbol of wTron is depicted in Fig. 4(h). While an nTron can be fabricated at the sub-100 nm scale, enabling monolithic integration with SNSPDs, a wTron is typically fabricated at the micrometer scale, making it compatible with SFQ-based fabrication processes. For example, wTron devices have been fabricated in MIT Lincoln Lab SFQ5ee process in [180]. The larger dimensions of a wTron

enable it to drive high capacitive loads (up to 500 pF) typical of semiconductor (CMOS) circuits [180].

2) **Superconductor-based transistor:** While cryotrons function primarily as digital switches, several superconductor-based devices exhibit analog behavior analogous to that of semiconductor transistors. Examples include the quiteron [187], [188], superconducting field-effect transistor (FET) [189], superconducting-ferromagnetic transistor [190]–[193], Josephson FET [194]–[196], superconducting Dayem bridge FET [197], metallic supercurrent FET [198], and superconducting quantum interference proximity transistor [199]. Although there are currently no demonstrations of SFQ-based or SNSPD-based triggering of superconductor-based transistors, these devices have the potential to be integrated into more complex circuits and serve as second stage amplifiers, such as a low noise amplifier or a differential amplifier, similar to those used in semiconductor circuits [37], [38], [200]–[203]. Nevertheless, to the best of the authors' knowledge, no digital data link has yet been implemented using superconductor-based transistors.

IV. EFFECT OF FABRICATION TECHNOLOGY

In this section, the effects of different fabrication technology parameters on the performance of interface circuits are discussed. Particular attention is given to JJ-based output drivers and semiconductor amplifiers due to the widespread availability of various fabrication processes for these interface circuits.

A. JJ-based output drivers

JJ-based fabrication processes (such as MIT Lincoln Lab SFQ5ee [88], SEEQC SFQ-C5SL [89], ADP2 [90], SIMIT Nb03P [91], and FLUXONICS CJ2 [92]) are characterized primarily by the critical current density J_c . Typical values of J_c range from 10 to 100 $\mu\text{A}/\mu\text{m}^2$. The switching speed of JJs scales approximately with the square root of the critical current density, J_c , [151]. For example, increasing the critical current density J_c from 10 $\mu\text{A}/\mu\text{m}^2$ to 100 $\mu\text{A}/\mu\text{m}^2$ results in approximately a 3.16-fold increase in switching speed. Therefore, processes with higher J_c values (e.g., 100 $\mu\text{A}/\mu\text{m}^2$) are preferred for high-speed applications of JJ-based drivers, such as SQUID stacks and SFQ-to-DC converters.

In addition to the switching speed, the output voltage of overdamped JJs also scales approximately with the square root of J_c [151]. SQUID-based output drivers should be fabricated using a high J_c process to maximize the output voltage swing. The output voltage of latching drivers (with underdamped JJs) depends on the gap voltage V_g , which is relatively consistent across modern fabrication processes and typically ranges from 2.6 to 2.8 mV.

Low-power applications such as superconducting qubit control and readout often use processes with lower J_c [89], [164]. For instance, an SFQ-to-DC converter fabricated using the AIST 2.5 $\mu\text{A}/\mu\text{m}^2$ process dissipates 74 nW of power, which is approximately two orders of magnitude lower than that of a comparable SFQ-to-DC converter designed with MIT Lincoln Lab 100 $\mu\text{A}/\mu\text{m}^2$ process [71].

The majority of JJ-based output drivers incorporate explicit inductors (*i.e.*, not parasitic inductors) in their circuit design, as illustrated in Fig. 2. Additionally, low-power biasing schemes such as ERSFQ and eSFQ, applicable to SQUID-based output drivers, employ large bias inductors on the order of hundreds of picohenries [6], [7]. These inductors require a significant layout footprint, thereby limiting the scalability of output drivers. Inductor-less superconductor electronic circuits have been proposed in the literature, utilizing conventional and bistable JJs (*e.g.*, 2- ϕ JJ) [166], [204]–[208]. Similar approaches could be applied to SQUID-based output drivers to reduce or potentially eliminate the need for inductors. However, since bistable JJs incorporate ferromagnetic materials, the corresponding fabrication processes remain immature for large-scale circuit integration [208].

Latching output drivers are sensitive to the parasitic capacitance to ground (C_g) associated with each JJ. A lower C_g is preferred in these drivers to minimize delay and reset time [209]. In Suzuki stack interface circuits, the ground plane underneath the drivers is removed to reduce C_g , as suggested in [99].

JJ-based output drivers are typically designed to operate at 4 K or below due to the Nb-based fabrication process, which has a critical temperature around 9 K. A high-temperature superconductor (HTS)-based fabrication process, which uses YBCO and LSAT materials, has been used to fabricate latching output drivers in [110], [119], [210]. To achieve an underdamped behavior, the JJs are shunted with capacitors, and a J_c of 200 $\mu\text{A}/\mu\text{m}^2$ is used to reduce the punchthrough probability of JJs [110]. In [110], a 4-JJ Suzuki stack circuit produces 1.0 mV at 30 K. The measured output voltage is smaller than expected (*i.e.*, only one of the JJs in the stack is turned on), which could be caused by the greater than 30% spread of the critical current of JJs [110]. Further optimization of the HTS-based process is required to reduce the spread of critical current [110]. Superconducting output drivers operating at intermediate temperature stages (*e.g.*, 10–50 K) could significantly improve the cooling power budget of the cryostat as compared to semiconductor amplifiers.

B. Semiconductor amplifiers

Semiconductor amplifiers in cryogenic digital data links are typically implemented using CMOS or bipolar CMOS (BiCMOS) technologies. CMOS-based amplifiers have been used in 4 K Josephson-CMOS hybrid memories, as reported in [37], [38]. High-frequency data links from 4 K to room-temperature electronics utilize BiCMOS-based amplifiers, which can provide faster switching speed (*i.e.*, data rate), and higher gain and output drive current as compared to CMOS technology. Examples of SiGe BiCMOS amplifiers have been demonstrated in [200]–[203].

Existing demonstrations of cryogenic semiconductor amplifiers within digital data links often utilize mature fabrication nodes such as 180 nm CMOS [37], [211], [212], 65 nm CMOS [155], and 130 nm BiCMOS [200]–[203] primarily due to relatively low fabrication costs. Konno *et al.* [37] discuss the possibility of using modern fabrication nodes ranging

from 22 nm to 7 nm FinFET technology to reduce power dissipation and improve switching speed in Josephson-CMOS memory systems, which include semiconductor amplifiers. Additionally, the threshold voltage of MOSFETs reduces in more advanced process nodes [213]. By lowering the threshold voltage of the second stage semiconductor amplifier, the required output voltage of the first stage superconducting output driver can be reduced, leading to lower overall power dissipation.

A hybrid amplifier that uses both CMOS and JJ devices was proposed in 1993 by Ghoshal *et al.* [214]. This hybrid amplifier employs an inverter circuit comprising an NMOS transistor and a series stack of JJs, which together replace the PMOS transistor [214]. The JJ stack provides a negative differential resistance and reduces the required time to charge the load capacitor [214], [215]. Additionally, this JJ stack eliminates the Miller effect [214], [215]. Similar hybrid amplifiers have been presented in [117], [123]. An experimental demonstration of a hybrid amplifier (with three NMOS transistors and 400-JJ stack) has been presented in [124], where CMOS and Josephson chips have been fabricated separately and interconnected via solder-bump bonding.

V. COMPARISON OF SUPERCONDUCTING OUTPUT DRIVERS

In this section, the superconducting output drivers are compared based on circuit- and system-level parameters. Particularly, the parameters such as output voltage, data rate, power dissipation, layout area, heat (thermal) load of cryogenic cables, line coding scheme, flux trapping, bit-error rate, and hardware security are considered.

A. Circuit-level parameters

Due to the stringent cooling power constraints at cryogenic temperatures, the superconducting output drivers with higher data rate and greater output voltage are highly desirable. A higher data rate per channel reduces the number of cryogenic interconnects required. A higher output voltage from the first stage output driver enables the second stage semiconductor amplifier to operate with lower gain and reduced power dissipation. A comparison of superconducting output drivers in terms of output voltage and data rate parameters, as reported in the literature over the past 40–50 years, is shown in Fig. 5(a). As summarized in the figure, no output driver has demonstrated both high output voltage and high data rate concurrently. Therefore, there is a trade-off between the output voltage and the data rate. For example, Suzuki stacks deliver output voltages on the order of tens to hundreds of mV and operate at data rates of a few Gbps. In contrast, SQUID stacks achieve data rates of 20–30 Gbps with output voltages below 10 mV. Cryotron-based devices deliver the highest output voltages, exceeding 1 V, but operate at data rates below 1 Gbps. SFQ-to-DC converters produce the lowest output voltages, around 1 mV, while supporting the highest data rates of up to 40–50 Gbps.

In addition to output voltage and data rate, power dissipation and layout area are critical factors in evaluating output drivers.

Lower power dissipation is desirable to maximize the available cooling power and support a higher number of interface channels. Layout area is particularly important for SFQ-based chips, where current fabrication processes impose limitations on integration density. Fig. 5(b) summarizes the key trends in these parameters. The power dissipation of Suzuki and SQUID stack drivers is the highest and exceeds 100 μ W per channel. Although Suzuki stack has a significantly lower number of JJs as compared to SQUID stack, this driver has a large bias resistor (see R_b in Fig. 2(d)), which is needed to maintain the high output voltage during switching [99]. R_b contributes to both power dissipation and layout area [99], [120] and could possibly be reduced with a DC-biased scheme and by adding a large bias inductor as suggested in [132]. The power dissipation of a SQUID stack (and other SQUID-based output driver) depends on the type of SFQ logic being used. For example, RSFQ logic family has large static power dissipation due to the resistive bias scheme [1]. Energy-efficient variants such as the RQL-based SQUID stack has lower power dissipation on the order of sub- μ W, as demonstrated in [156]. Fig. 5(c) and Fig. 5(d) present comparisons of superconducting output drivers based on a figure of merit (FOM), layout area, and output voltage. This FOM, proposed by Gupta *et al.* [71], is defined as the ratio of power dissipation to data rate. Each category of output drivers (see taxonomy in Fig. 1(b)) is represented as a distinct group in Fig. 5(c) and Fig. 5(d). From Fig. 5(d), the trade-off between output voltage and the figure of merit (FOM) is clearly observed for JJ-based output drivers. Specifically, higher output voltages correspond to higher FOM values, that is, increased power dissipation and/or reduced data rates.

B. Heat load of cryogenic cables

Cryogenic bias and signal cables contribute a significant amount of heat (thermal) load, which reduces the cooling power available for the cryostat payload [216], [217]. Depending on the type of power supply (*i.e.* AC or DC), different cryogenic cables are preferred. Coaxial cables are typically used for AC bias, whereas twisted pair cables are used for DC bias power supply [132]. The heat load of AC-bias cables is generally higher as compared to the DC-bias cables [130]. For instance, Mustafa *et al.* [132] compared the heat load of the bias cables for AC- and DC-biased 4JL gates and Suzuki stack circuits. AC-bias cables have approximately three orders of magnitude higher heat load as compared to the DC-biased cables (*e.g.*, for a 30-channel Suzuki stack interface, an AC-bias cable has 66.0 μ W, and a DC-bias cable has 34.6 nW) [132]. The type of biasing (AC and/or DC) for different superconducting output drivers is listed in Fig. 5(b).

The cryogenic signal cables are used to transmit the digital data from the superconducting output drivers. Several BeCu-Cu-BeCu stripline ribbon cables, which are employed for 4 K to room-temperature data transmission, have been analyzed and compared in [71]. These cables have a 4 K heat load of 440 μ W per line at 2.1 Gbps, 740 μ W per line at 5.7 Gbps, and 1118 μ W per line at 10.0 Gbps. Additionally, BeCu coaxial cables have been reported with 2473 μ W per line at 42.9 Gbps [71]. Superconducting output drivers have two types of output

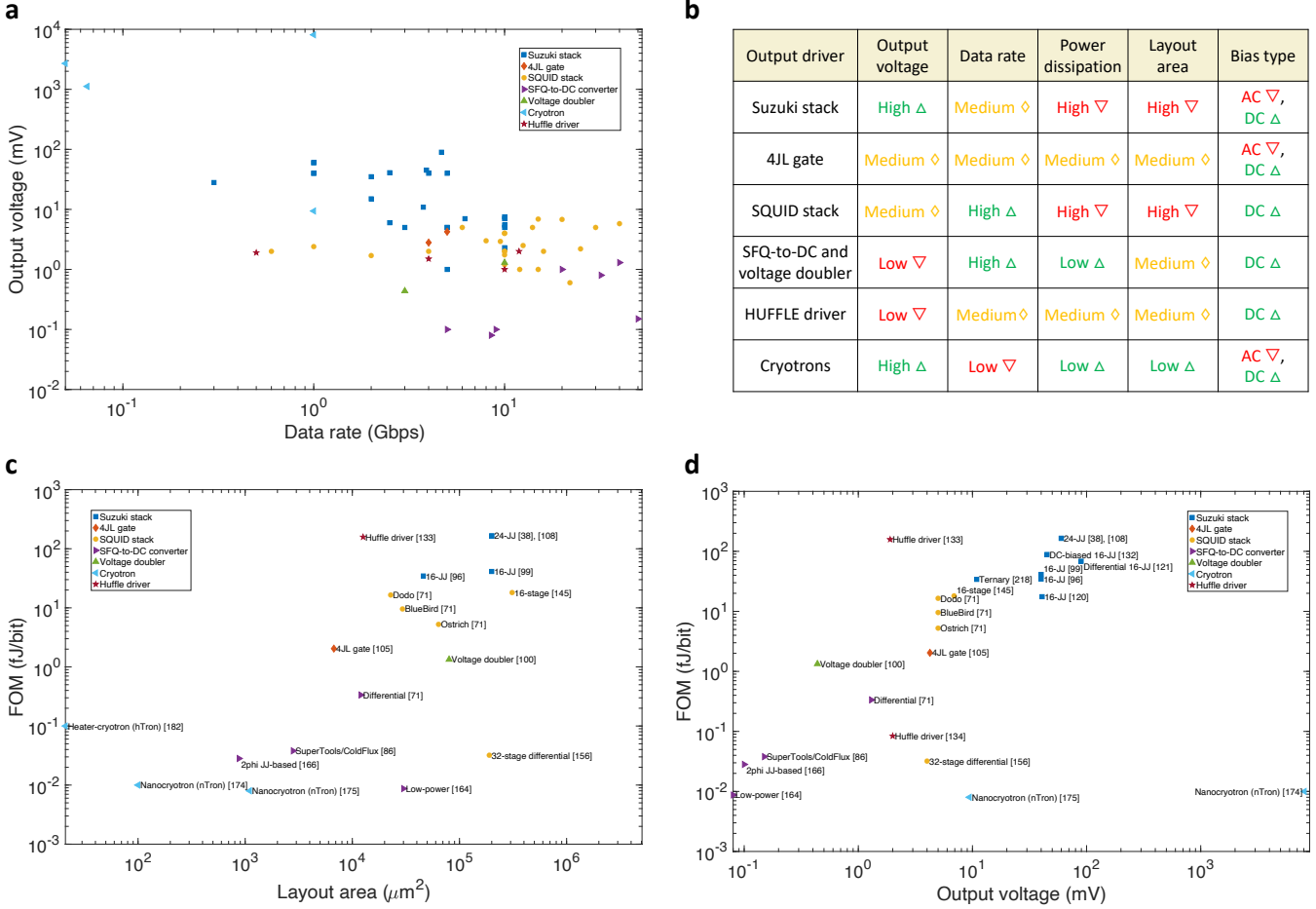


Fig. 5. Comparison of superconducting output drivers. **a**, Output voltage and data rate parameters comparison. **b**, General trends in output voltage, data rate, power dissipation, layout area, and bias type. Green, orange, and red colors (Δ , \diamond , and ∇ symbols) correspond to desired, intermediate, and undesired performance, respectively. **c**, FOM and layout area parameters comparison. **d**, FOM and output voltage parameters comparison. FOM is calculated as power dissipation (only circuit-level component) divided by data rate.

signaling: single-ended and differential. Differential signaling offers a larger output voltage swing and improved noise immunity due to the common-mode rejection property [71]. Superconducting output drivers with differential signaling have been proposed in the literature including implementations based on SQUID stacks [71], [151], SFQ-to-DC converters [71], [151], and Suzuki stacks [121]. The single-ended and differential output drivers require one and two output cables, respectively. As a result, the heat load of a differential output driver is approximately twice that of a single-ended driver [71].

C. Line coding schemes

Superconducting output drivers typically employ binary data transmission. A binary bit string is encoded with either NRZ-M (non-return-to-zero mark) or RZ (return-to-zero) line coding schemes. In the NRZ-M scheme, the output signal is toggled from high-to-low or low-to-high voltage state when a logical ‘1’ is transmitted. A logical ‘0’ corresponds to no transition, where the previous voltage state is maintained. The NRZ-M scheme is commonly used in SQUID-based output drivers such as the SQUID stack, SFQ-to-DC converter, and voltage doubler, as shown in Fig. 3(a)-(c). Additionally, the HUFFLE

driver can produce an NRZ-M signaling (Fig. 3(d)). Other types of output drivers (*e.g.*, latching and cryotrons) typically employ the RZ scheme, where the logical ‘1’ produces a high voltage state for the first half of the clock period and returns to zero voltage state in the second half. A logical ‘0’ is represented as the low output voltage for the entire clock period. The RZ line coding of Suzuki stack and 4JL gate circuits can be observed in Fig. 3(e) and Fig. 3(f), respectively.

SQUID-based output drivers can also be operated in the RZ line coding scheme by utilizing a delay element as demonstrated in [97]. However, the NRZ scheme is generally preferred in high-speed digital data links because it provides better signal quality at higher data rates as compared to the RZ scheme [140], [170].

Multi-level signal transmission increases the effective data rate by encoding more than one bit per clock cycle. A ternary superconducting output driver has been proposed in [218]. This ternary driver builds upon a re-designed Suzuki stack circuit with three arrays of serially connected JJs and can produce three output voltage levels [218]. For a fixed clock frequency, the ternary digital data link can increase the effective data rate by 50% as compared to a binary data

link [218]. Alternatively, a ternary link can potentially reduce the number of cryogenic cables by 33% while maintaining the same effective data rate [218]. A similar concept of a multi-level output driver has been proposed in [103], where the SQUID stack circuit is configured to produce a 4-level pulse-amplitude modulated (PAM-4) signal. With four output voltage levels, the effective data rate can be doubled [103]. The PAM-4 signals generated by the SQUID stack driver can be directly interfaced with modern cryogenic FPGAs (*e.g.*, Xilinx Artix-7), memory (*e.g.*, Micron's GDDR6X), and serial links (*e.g.*, Intel's CEI-56G), all of which support PAM-based communication protocols [103].

D. Flux trapping

Superconductor digital circuits are susceptible to flux trapping caused by external magnetic fields, which occurs when magnetic flux becomes pinned in defects or inhomogeneities within the superconducting material. This trapped flux can lead to localized disruptions in superconductivity, resulting in performance degradation or circuit failure [219], [220]. This effect may occur in SQUID-based, HUFFLE, and 4JL gate output drivers due to the superconducting loops in their implementations (Fig. 2). As previously mentioned, a Suzuki stack driver incorporates two small resistors R_{br} (see Fig. 2(d)), which prevent flux trapping [99]. Cryotron devices do not have superconducting loops and, therefore, are not susceptible to flux trapping.

E. Bit-error rate (BER)

Bit errors within digital data links can arise from fabrication defects, process parameter variations, flux trapping, signal attenuation, and noise. The bit-error rate (BER) is determined by dividing the number of bit-errors by the total number of transmitted bits. State-of-the-art output drivers based on SQUID stacks (data rate of 10-20 Gbps) [71], [97], [142], SFQ-to-DC converters (data rate of 18 Gbps) [71], and Suzuki stacks (data rate of 1-5 Gbps) [99], [108], [116], [125] have demonstrated BER below 10^{-12} . The early implementation of nTron-based output driver has the BER of 4×10^{-4} operating at around 100 Mbps [175].

Error-correction codes can be utilized to detect and correct bit errors. Linear block codes have been proposed for superconducting output drivers in [221], [222]. By employing, *e.g.*, a (32,32) linear block code, BER can be reduced by at least three orders of magnitude [221].

F. Hardware security

Hardware security of integrated circuits is a research field dedicated to uncovering hardware-level vulnerabilities and preventing malicious activities such as intellectual property piracy, reverse engineering, covert communication, and side-channel attacks. Unlike software-level attacks, hardware security vulnerabilities are more difficult to mitigate once the chip has been fabricated and released to market. Therefore, hardware security should be considered during the design of integrated circuits along with power, performance, area, and cost metrics.

One of the most prominent threats in hardware security comes from side-channel attacks. Side-channel attacks monitor the tiny variations in, *e.g.*, power supply, and are able to infer the internal circuit switching. A considerable amount of side-channel leakage has been identified in superconducting output drivers as compared to standard SFQ circuits [223]–[225]. By measuring the power supply from room-temperature electronics, it is possible to decode the bits, which are transmitted by superconducting output drivers, without physically touching the output signal pads [223]. Significant fluctuations in the bias current on the order of tens to hundreds of μA have been identified in SFQ-to-DC converters, SQUID stacks, and Suzuki stack output drivers [225].

Since it is possible to obtain the information from power supply variations, one may use the side-channel leakage information for cryogenic testing and verification purposes, as proposed in [226]. In this approach, superconducting output drivers are connected to a common power supply, generating a measurable side-channel leakage [226]. The output voltage terminals are not connected to the output pads, which significantly reduces the thermal load (*i.e.*, there are no cryogenic cables connected to the output signals).

VI. CONCLUSION AND OUTLOOK

In this work, a detailed review of superconductor-semiconductor interface circuits is presented. A particular focus is placed on superconducting output drivers that can convert and amplify SFQ pulses to DC voltage signals to be processed by semiconductor circuits. Two main categories of superconducting output drivers are identified such as JJ-based drivers and multi-terminal devices. The working principle, advantages, and limitations are discussed for various types of interface circuits that have been proposed in the past 40-50 years. A comprehensive comparison of these interface circuits demonstrates the trade-offs among several design parameters including output voltage, data rate, power dissipation, layout area, power supply type (AC or DC), and BER. The selection of an appropriate interface circuit requires thorough evaluation and depends on the design requirements for specific applications such as HPC, superconducting quantum computing, digital signal processing, single-photon detection, and neuromorphic computing. With continuous improvements in fabrication processes, it is important to consider key parameters that influence the performance of specific interface circuits. This survey presents such an analysis focusing on JJ-based output drivers and semiconductor amplifiers. Due to the relatively recent introduction of multi-terminal devices and their ongoing development, further research is necessary to understand the implications of various fabrication processes on multi-terminal superconducting output drivers. Furthermore, the development of interface circuits that leverage novel ferromagnetic JJs, which exhibit bistable behavior, and superconductor-based transistors needs future research.

ACKNOWLEDGMENT

The authors would like to thank D. Scott Holmes for fruitful discussions.

REFERENCES

[1] K. K. Likharev and V. K. Semenov, "RSFQ logic/memory family: A new Josephson-junction technology for sub-terahertz-clock-frequency digital systems," *IEEE Transactions on Applied Superconductivity*, vol. 1, no. 1, pp. 3–28, March 1991, DOI: 10.1109/77.80745.

[2] D. S. Holmes, A. L. Ripple, and M. A. Manheimer, "Energy-efficient superconducting computing—power budgets and requirements," *IEEE Transactions on Applied Superconductivity*, vol. 23, no. 3, June 2013, Art. no. 1701610, DOI: 10.1109/TASC.2013.2244634.

[3] J. X. Przybysz, D. L. Miller, H. Toepfer, O. Mukhanov, J. Lisenfeld, M. Weides, H. Rotzinger, and P. Febvre, "Superconductor digital electronics," *Applied Superconductivity: Handbook on Devices and Applications*, pp. 1111–1206, 2015, DOI: 10.1016/j.physc.2012.05.016.

[4] A. I. Braginski, "Superconductor electronics: Status and outlook," *Journal of Superconductivity and Novel Magnetism*, vol. 32, no. 1, pp. 23–44, November 2019, DOI: 10.1007/s10948-018-4884-4.

[5] G. Krylov, T. Jabbari, and E. G. Friedman, *Single Flux Quantum Integrated Circuit Design, Second Edition*. Springer, 2024.

[6] D. Kirichenko, S. Sarwana, and A. Kirichenko, "Zero static power dissipation biasing of RSFQ circuits," *IEEE Transactions on Applied Superconductivity*, vol. 21, no. 3, pp. 776–779, June 2011, DOI: 10.1109/TASC.2010.2098432.

[7] O. A. Mukhanov, "Energy-efficient single flux quantum technology," *IEEE Transactions on Applied Superconductivity*, vol. 21, no. 3, pp. 760–769, June 2011, DOI: 10.1109/TASC.2010.2096792.

[8] Q. P. Herr, A. Y. Herr, O. T. Oberg, and A. G. Ioannidis, "Ultra-low-power superconductor logic," *Journal of Applied Physics*, vol. 109, no. 10, May 2011, Art. no. 103903, DOI: 10.1063/1.3585849.

[9] N. Takeuchi, D. Ozawa, Y. Yamanashi, and N. Yoshikawa, "An adiabatic quantum flux parametron as an ultra-low-power logic device," *Superconductor Science and Technology*, vol. 26, no. 3, January 2013, Art. no. 035010, DOI: 10.1088/0953-2048/26/3/035010.

[10] Q. Herr, T. Josephsen, and A. Herr, "Superconducting pulse conserving logic and Josephson-SRAM," *Applied Physics Letters*, vol. 122, no. 18, May 2023, Art. no. 182604, DOI: 10.1063/5.0148235.

[11] F. V. Lupo, O. A. Mukhanov, and M. Arzeo, "Digital phase source for Josephson junction computing," March 2025, US Patent App. 18/822,229, Link.

[12] Y. Ando, R. Sato, M. Tanaka, K. Takagi, N. Takagi, and A. Fujimaki, "Design and demonstration of an 8-bit bit-serial RSFQ microprocessor: CORE e4," *IEEE Transactions on Applied Superconductivity*, vol. 26, no. 5, August 2016, Art. no. 1301205, DOI: 10.1109/TASC.2016.2565609.

[13] K. Ishida, M. Tanaka, T. Ono, and K. Inoue, "Towards ultra-high-speed cryogenic single-flux-quantum computing," *IEICE Transactions on Electronics*, vol. 101, no. 5, pp. 359–369, May 2018, DOI: 10.1587/transe.E101.C.359.

[14] C. L. Ayala, T. Tanaka, R. Saito, M. Nozoe, N. Takeuchi, and N. Yoshikawa, "MANA: A monolithic adiabatic integration architecture microprocessor using 1.4-zJ/op unshunted superconductor Josephson junction devices," *IEEE Journal of Solid-State Circuits*, vol. 56, no. 4, pp. 1152–1165, April 2021, DOI: 10.1109/JSSC.2020.3041338.

[15] R. Kashima, I. Nagaoka, M. Tanaka, T. Yamashita, and A. Fujimaki, "64-GHz datapath demonstration for bit-parallel SFQ microprocessors based on a gate-level-pipeline structure," *IEEE Transactions on Applied Superconductivity*, vol. 31, no. 5, August 2021, DOI: 10.1109/TASC.2021.3061353.

[16] I. Nagaoka, R. Kashima, T. Nakano, M. Tanaka, T. Yamashita, K. Inoue, and A. Fujimaki, "A 57.2 GHz 11.2 mW 8-bit general purpose superconductor microprocessor with dual-clocking scheme," in *IEEE Asian Solid-State Circuits Conference (A-SSCC)*, November 2022, pp. 1–3, DOI: 10.1109/A-SSCC56115.2022.9980802.

[17] M. Tanaka, R. Saito, A. Fujimaki, K. Takagi, and N. Takagi, "Execution of stored programs by a rapid single-flux-quantum random-access-memory-embedded bit-serial microprocessor using 50-GHz clock frequency," *Applied Physics Letters*, vol. 122, no. 19, May 2023, Art. no. 192601, DOI: 10.1063/5.0148273.

[18] A. Herr and Q. Herr, "A data center in a shoebox: Imec's plan to use superconductors to shrink computers," *IEEE Spectrum*, vol. 61, no. 6, pp. 37–41, June 2024, DOI: 10.1109/MSPEC.2024.10551792.

[19] J. Kundu, D. Bhattacharjee, N. Josephsen, A. Pokhrel, U. De Silva, W. Guo, S. Van Winckel, S. Brebels, Q. Herr, A. Herr *et al.*, "A system level performance evaluation for superconducting digital systems," in *Design, Automation & Test in Europe Conference (DATE)*, March 2025, pp. 1–7, DOI: 10.23919/DATE64628.2025.10992879.

[20] E. B. Wikborg, V. K. Semenov, and K. K. Likharev, "RSFQ front-end for a software radio receiver," *IEEE Transactions on Applied Superconductivity*, vol. 9, no. 2, pp. 3615–3618, June 1999, DOI: 10.1109/77.783811.

[21] A. Kirichenko, S. Sarwana, D. Gupta, and D. Yohannes, "Superconductor digital receiver components," *IEEE Transactions on Applied Superconductivity*, vol. 15, no. 2, pp. 249–254, June 2005, DOI: 10.1109/TASC.2005.849771.

[22] D. Gupta, T. V. Filippov, A. F. Kirichenko, D. E. Kirichenko, I. V. Vernik, A. Sahu, S. Sarwana, P. Shevchenko, A. Talalaevskii, and O. A. Mukhanov, "Digital channelizing radio frequency receiver," *IEEE Transactions on applied superconductivity*, vol. 17, no. 2, pp. 430–437, June 2007, DOI: 10.1109/TASC.2007.898255.

[23] O. A. Mukhanov, D. Kirichenko, I. V. Vernik, T. V. Filippov, A. Kirichenko, R. Webber, V. Dotsenko, A. Talalaevskii, J. C. Tang, A. Sahu *et al.*, "Superconductor digital-RF receiver systems," *IEICE Transactions on Electronics*, vol. 91, no. 3, pp. 306–317, March 2008, DOI: 10.1093/ietele/e91-c.3.306.

[24] R. McDermott and M. Vavilov, "Accurate qubit control with single flux quantum pulses," *Physical Review Applied*, vol. 2, no. 1, July 2014, Art. no. 014007, DOI: 10.1103/PhysRevApplied.2.014007.

[25] U. Patel, I. V. Pechenezhskiy, B. Plourde, M. Vavilov, and R. McDermott, "Phonon-mediated quasiparticle poisoning of superconducting microwave resonators," *Physical Review B*, vol. 96, no. 22, December 2017, Art. no. 220501, DOI: 10.1103/PhysRevB.96.220501.

[26] R. McDermott, M. G. Vavilov, B. L. T. Plourde, F. K. Wilhelm, P. J. Liebermann, O. A. Mukhanov, and T. A. Ohki, "Quantum-classical interface based on single flux quantum digital logic," *Quantum science and technology*, vol. 3, no. 2, January 2018, Art. no. 024004, DOI: 10.1088/2058-9565/aaa3a0.

[27] O. Mukhanov, A. Kirichenko, C. Howington, J. Walter, M. Hutchings, I. Vernik, D. Yohannes, K. Dodge, A. Ballard, B. Plourde *et al.*, "Scalable quantum computing infrastructure based on superconducting electronics," in *IEEE International Electron Devices Meeting (IEDM)*. IEEE, December 2019, pp. 31.2.1–31.2.4, DOI: 10.1109/IEDM19573.2019.8993634.

[28] M. R. Jokar, R. Rines, G. Pasandi, H. Cong, A. Holmes, Y. Shi, M. Pedram, and F. T. Chong, "DigiQ: A scalable digital controller for quantum computers using SFQ logic," in *IEEE International Symposium on High-Performance Computer Architecture (HPCA)*. IEEE, April 2022, pp. 400–414, DOI: 10.1109/HPCA53966.2022.00037.

[29] C.-H. Liu, A. Ballard, D. Olaya, D. R. Schmidt, J. Biesecker, T. Lucas, J. Ullom, S. Patel, O. Rafferty, A. Opremcak *et al.*, "Single flux quantum-based digital control of superconducting qubits in a multichip module," *PRX Quantum*, vol. 4, no. 3, July 2023, Art. no. 030310, DOI: 10.1103/PRXQuantum.4.030310.

[30] J. Barbosa, J. C. Brennan, A. Casaburi, M. Hutchings, A. Kirichenko, O. Mukhanov, and M. Weides, "RSFQ all-digital programmable multitone generator for quantum applications," *IEEE Transactions on Quantum Engineering*, vol. 6, December 2024, Art. no. 5500211, DOI: 10.1109/TQE.2024.3520805.

[31] L. Di Palma, A. Miano, P. Mastrovito, D. Massarotti, M. Arzeo, G. P. Pepe, F. Tafuri, and O. Mukhanov, "Discriminating the phase of a coherent tone with a flux-switchable superconducting circuit," *Physical Review Applied*, vol. 19, no. 6, June 2023, Art. no. 064025, DOI: 10.1103/PhysRevApplied.19.064025.

[32] L. Di Palma, P. Mastrovito, A. Miano, A. Salim, F. Lupo, J. Bernhardt, L. Di Marino, D. Massarotti, G. Pepe, F. Tafuri *et al.*, "Fast digital phase detection of a coherent tone at GHz frequencies," *IEEE Transactions on Applied Superconductivity*, vol. 34, no. 3, May 2024, Art. no. 1300305, DOI: 10.1109/TASC.2024.3354681.

[33] L. Di Marino, L. Di Palma, M. Riccio, M. Arzeo, and O. Mukhanov, "Control of a Josephson digital phase detector via an SFQ-based flux bias driver," *IEEE Transactions on Quantum Engineering*, vol. 6, June 2025, Art. no. 3101708, DOI: 10.1109/TQE.2025.3583570.

[34] J. Bernhardt, C. Jordan, J. Rahamim, A. Kirchenko, K. Bharadwaj, L. Fry-Bouriaux, K. Porsch, A. Somoroff, K.-T. Tsai, J. Walter *et al.*, "Quantum computer controlled by superconducting digital electronics at millikelvin temperature," *arXiv preprint arXiv:2503.09879*, March 2025, DOI: 10.48550/arXiv.2503.09879.

[35] S. Nagasawa, Y. Hashimoto, H. Numata, and S. Tahara, "A 380 ps, 9.5 mW Josephson 4-Kbit RAM operated at a high bit yield," *IEEE Transactions on Applied Superconductivity*, vol. 5, no. 2, pp. 2447–2452, June 1995, DOI: 10.1109/77.403086.

[36] S. Nagasawa, T. Satoh, K. Hinode, Y. Kitagawa, and M. Hidaka, "Yield evaluation of 10- kA/cm^2 Nb multi-layer fabrication process using conventional superconducting RAMs," *IEEE Transactions on*

Applied Superconductivity, vol. 17, no. 2, pp. 177–180, June 2007, DOI: 10.1109/TASC.2007.898050.

[37] G. Konno, Y. Yamanashi, and N. Yoshikawa, “Fully functional operation of low-power 64-kb Josephson-CMOS hybrid memories,” *IEEE Transactions on Applied Superconductivity*, vol. 27, no. 4, June 2017, Art. no. 1300607, DOI: 10.1109/TASC.2016.2646911.

[38] T. Van Duzer, L. Zheng, S. Whiteley, H. Kim, J. Kim, X. Meng, and T. Ortlepp, “64-kb hybrid Josephson-CMOS 4 K random-access memory with 12 mW read power and 400 ps access time,” *IEEE Transactions on Applied Superconductivity*, vol. 23, no. 3, June 2013, Art. no. 1700504, DOI: 10.1109/TASC.2012.2230294.

[39] Y. Hironaka, Y. Yamanashi, and N. Yoshikawa, “Demonstration of a single-flux-quantum microprocessor operating with Josephson-CMOS hybrid memory,” *IEEE Transactions on Applied Superconductivity*, vol. 30, no. 7, October 2020, Art. no. 1301206, DOI: 10.1109/TASC.2020.2994208.

[40] S. Alam, M. S. Hossain, S. R. Srinivasa, and A. Aziz, “Cryogenic memory technologies,” *Nature Electronics*, vol. 6, no. 3, pp. 185–198, March 2023, DOI: 10.1038/s41928-023-00930-2.

[41] “Reuters: Snowcap Compute raises \$23 million for superconducting AI chips,” June 2025, Link.

[42] “We’re scaling quantum computing even faster with Atlantic Quantum.,” Oct. 2, 2025, Link.

[43] B. KANNAN, Y. Sung, L. C. Ding, T. Menke, S. S. Novikov, S. K. F. Gustavsson, and W. D. Oliver, “Managing coupling in a quantum computing system,” April 2024, US Patent App. 18/477,603, Link.

[44] “Quantum Insider: SEEQC Develops Digital Interface for Real-Time Quantum-Classical Integration with NVIDIA-Powered Error Correction,” March 2025, Link.

[45] “SEEQC Announces Digital Chip-Based Collaboration with NVIDIA to Accelerate Quantum Supercomputing.,” Accessed: Aug 14, 2025, Link.

[46] J. MITOLA III, “Software radio architecture evolution: Foundations, technology tradeoffs, and architecture implications,” *IEICE Transactions on Communications*, vol. 83, no. 6, pp. 1165–1173, June 2000.

[47] “Advanced Digital-RF Receiver (ADR),” Accessed: Oct 23, 2025, Link.

[48] G. Gol’Tsman, O. Okunev, G. Chulkova, A. Lipatov, A. Semenov, K. Smirnov, B. Voronov, A. Dzardanov, C. Williams, and R. Sobolewski, “Picosecond superconducting single-photon optical detector,” *Applied Physics Letters*, vol. 79, no. 6, pp. 705–707, August 2001, DOI: 10.1063/1.1388868.

[49] C. M. Natarajan, M. G. Tanner, and R. H. Hadfield, “Superconducting nanowire single-photon detectors: physics and applications,” *Superconductor Science and Technology*, vol. 25, no. 6, April 2012, Art. no. 063001, DOI: 10.1088/0953-2048/25/6/063001.

[50] R. Hummatov, A. E. Lita, T. Farrahi, N. Otoooshi, S. Fayer, M. J. Collins, M. Durkin, D. Bennett, J. Ullom, R. P. Mirin *et al.*, “Fast transition-edge sensors suitable for photonic quantum computing,” *Journal of Applied Physics*, vol. 133, no. 23, June 2023, Art. no. 234502, DOI: 10.1063/5.0149478.

[51] L. Gottardi and K. Nagayashi, “A review of X-ray microcalorimeters based on superconducting transition edge sensors for astrophysics and particle physics,” *Applied Sciences*, vol. 11, no. 9, April 2021, Art. no. 3793, DOI: 10.3390/app11093793.

[52] J. N. Ullom and D. A. Bennett, “Review of superconducting transition-edge sensors for x-ray and gamma-ray spectroscopy,” *Superconductor Science and Technology*, vol. 28, no. 8, July 2015, Art. no. 084003, DOI: 10.1088/0953-2048/28/8/084003.

[53] “International Electrotechnical Commission (IEC) 61788-22-3,” August 2022, Link.

[54] S. Miyajima, S. Miki, M. Yabuno, T. Yamashita, and H. Terai, “Timing discriminator based on single-flux-quantum circuit toward high time-resolved photon detection,” *Superconductor Science and Technology*, vol. 30, no. 12, p. 12LT01, October 2017, DOI: 10.1088/1361-6668/aa926e.

[55] S. Miki, S. Miyajima, M. Yabuno, T. Yamashita, T. Yamamoto, N. Imoto, R. Ikuta, R. Kirkwood, R. Hadfield, and H. Terai, “Superconducting coincidence photon detector with short timing jitter,” *Applied Physics Letters*, vol. 112, no. 26, June 2018, Art. no. 262601, DOI: 10.1063/1.5037254.

[56] C. D. Shelly, P. See, E. J. Romans, A. Casaburi, J. Ireland, J. M. Williams, and R. H. Hadfield, “Modelling of a two-signal SFQ detection scheme for the readout of superconducting nanowire single photon detectors,” in *16th International Superconductive Electronics Conference (ISEC)*, June 2017, pp. 1–3, DOI: 10.1109/ISEC.2017.8314235.

[57] I. V. Komissarov, A. J. Salim, O. A. Mukhanov, T. Rambo, A. Miller, and R. Sobolewski, “Modified superconducting single-flux quantum two-photon coincidence correlator for single-photon measurements,” in *CLEO: Applications and Technology*. Optica Publishing Group, May 2024, pp. JW2A–89, DOI: 10.1364/CLEO_AT.2024.JW2A.89.

[58] R. Sobolewski, I. Komissarov, A. J. Salim, J. Walter, D. Yohannes, O. Mukhanov, A. Talalaevski, E. Track, T. Rambo, and A. Miller, “Electrical testing of SNSPD-SFQ two-photon coincidence correlator,” in *Quantum Optics and Photon Counting*. SPIE, June 2025, p. PC1352506, DOI: 10.1117/12.3059863.

[59] K. Zheng, Q.-Y. Zhao, L.-D. Kong, S. Chen, H.-Y.-B. Lu, X.-C. Tu, L.-B. Zhang, X.-Q. Jia, J. Chen, L. Kang *et al.*, “Characterize the switching performance of a superconducting nanowire cryotron for reading superconducting nanowire single photon detectors,” *Scientific Reports*, vol. 9, no. 1, November 2019, Art. no. 16345, DOI: 10.1038/s41598-019-52874-3.

[60] M. Castellani, O. Medeiros, R. A. Foster, A. Buzzi, M. Colangelo, J. C. Bienfang, A. Restelli, and K. K. Berggren, “Nanocryotron ripple counter integrated with a superconducting nanowire single-photon detector for megapixel arrays,” *Physical Review Applied*, vol. 22, no. 2, August 2024, Art. no. 024020, DOI: 10.1103/PhysRevApplied.22.024020.

[61] A. Bozbey, S. Miyajima, H. Akaike, and A. Fujimaki, “Single-flux-quantum circuit based readout system for detector arrays by using time to digital conversion,” *IEEE Transactions on Applied Superconductivity*, vol. 19, no. 3, pp. 509–513, June 2009, DOI: 10.1109/TASC.2009.2018038.

[62] S. W. Leman, E. B. Golden, M. C. Guyton, K. K. Ryu, and A. Wynn, “Integrated superconducting transition-edge-sensor energy readout (ISTER),” *IEEE Transactions on Applied Superconductivity*, vol. 33, no. 5, August 2023, Art. no. 2500807, DOI: 10.1109/TASC.2023.3271276.

[63] J. Beyer, P. De Korte, C. D. Reintsema, S. W. Nam, M. MacIntosh, G. Hilton, L. Vale, and K. Irwin, “Performance of 32-channel time-division SQUID multiplexer for cryogenic detector arrays,” *IEEE Transactions on Applied Superconductivity*, vol. 13, no. 2, pp. 649–652, June 2003, DOI: 10.1109/TASC.2003.813983.

[64] M. Durkin, J. S. Adams, S. R. Bandler, J. A. Chervenak, S. Chaudhuri, C. S. Dawson, E. V. Denison, W. B. Doriese, S. M. Duff, F. M. Finkbeiner *et al.*, “Demonstration of Athena X-IFU compatible 40-row time-division-multiplexed readout,” *IEEE Transactions on Applied Superconductivity*, vol. 29, no. 5, August 2019, Art. no. 2101005, DOI: 10.1109/TASC.2019.2904472.

[65] M. Kiviranta, L. Grönberg, T. Puranen, J. Van der Kuur, N. Beev, J. Salonen, D. Hazra, and S. Korpela, “Two-stage SQUID amplifier for the frequency multiplexed readout of the X-IFU X-ray camera,” *IEEE Transactions on Applied Superconductivity*, vol. 31, no. 5, August 2021, Art. no. 1600605, DOI: 10.1109/TASC.2021.3060356.

[66] M. Kiviranta and L. Grönberg, “Two-stage SQUID amplifier with bias current re-use,” *IEEE Transactions on Applied Superconductivity*, vol. 35, no. 5, August 2025, Art. no. 1600304, DOI: 10.1109/TASC.2024.3514594.

[67] M. Schneider, E. Toomey, G. Rowlands, J. Shainline, P. Tschirhart, and K. Segall, “SuperMind: a survey of the potential of superconducting electronics for neuromorphic computing,” *Superconductor Science and Technology*, vol. 35, no. 5, March 2022, Art. no. 053001, DOI: 10.1088/1361-6668/ac4cd2.

[68] M. M. Islam, S. Alam, M. S. Hossain, K. Roy, and A. Aziz, “A review of cryogenic neuromorphic hardware,” *Journal of Applied Physics*, vol. 133, no. 7, February 2023, Art. no. 070701, DOI: 10.1063/5.0133515.

[69] M. A. Karamuftuoglu, A. Bozbey, and S. Razmkhah, “JJ-Soma: Toward a spiking neuromorphic processor architecture,” *IEEE Transactions on Applied Superconductivity*, vol. 33, no. 8, November 2023, Art. no. 1400607, DOI: 10.1109/TASC.2023.3270766.

[70] S. Razmkhah, M. A. Karamuftuoglu, and A. Bozbey, “Hybrid synaptic structure for spiking neural network realization,” *Superconductor Science and Technology*, vol. 37, no. 6, May 2024, Art. no. 065011, DOI: 10.1088/1361-6668/ad44e3.

[71] D. Gupta, S. Sarwana, D. Kirichenko, V. Dotsenko, A. E. Lehmann, T. V. Filippov, W.-T. Wong, S.-W. Chang, P. Ravindran, and J. Bardin, “Digital output data links from superconductor integrated circuits,” *IEEE Transactions on Applied Superconductivity*, vol. 29, no. 5, August 2019, Art. no. 1303208, DOI: 10.1109/TASC.2019.2910469.

[72] K. Sakai, S. Kato, N. Yoshikawa, Y. Kokubun, and T. Arakawa, “Proposal of ultra-low voltage quantum well optical modulator for optical interconnection in superconducting integrated circuit systems,” *Japanese Journal of Applied Physics*, vol. 59, no. S0, April 2020, Art. no. SOOB01, DOI: 10.35848/1347-4065/ab8284.

[73] A. Youssefi, I. Shomroni, Y. J. Joshi, N. R. Bernier, A. Lukashchuk, P. Uhrich, L. Qiu, and T. J. Kippenberg, “A cryogenic electro-optic

interconnect for superconducting devices.” *Nature Electronics*, vol. 4, no. 5, pp. 326–332, May 2021, DOI: 10.1038/s41928-021-00570-4.

[74] M. de Cea and R. J. Ram, “Attojoule-per-bit electrical energy consumption optical modulators at 4 K and 300 K through energy harvesting,” in *IEEE Photonics Conference (IPC)*, October 2021, pp. 1–2, DOI: 10.1109/IPC48725.2021.9592911.

[75] P. Pintus, M. Soltani, and G. Moody, “Cryogenic optical data link for superconducting circuits,” *Nature Photonics*, vol. 18, no. 4, pp. 306–308, April 2024, DOI: 10.1038/s41566-024-01417-y.

[76] B. Yin, H. Gevorgyan, D. Onural, A. Khilo, M. A. Popović, and V. M. Stojanović, “Electronic-photonic cryogenic egress link,” in *IEEE 47th European Solid State Circuits Conference (ESSCIRC)*, September 2021, pp. 51–54, DOI: 10.1109/ESSCIRC53450.2021.9567813.

[77] M. Shen, J. Xie, Y. Xu, S. Wang, R. Cheng, W. Fu, Y. Zhou, and H. X. Tang, “Photonic link from single-flux-quantum circuits to room temperature,” *Nature Photonics*, vol. 18, no. 4, pp. 371–378, April 2024, DOI: 10.1038/s41566-023-01370-2.

[78] B. Yin, H. Gevorgyan, D. Onural, B. Zhang, A. Khilo, M. A. Popović, and V. M. Stojanović, “A fully packaged cryogenic optical transmitter directly interfaced with a superconducting chip,” *Nature Electronics*, pp. 1–6, January 2026, DOI: 10.1038/s41928-025-01505-z.

[79] O. Mukhanov, I. Vernik, A. Kirichenko, A. Kadin, K. D. Choquette, M. Tan, and T. Fryslie, “Development of energy-efficient cryogenic optical (ECO) data link,” in *IEEE 14th International Superconductive Electronics Conference (ISEC)*, July 2013, pp. 1–3, DOI: 10.1109/ISEC.2013.6604276.

[80] H. Wu, W. Fu, M. Feng, and D. Deppe, “2.6 K VCSEL data link for cryogenic computing,” *Applied Physics Letters*, vol. 119, no. 4, July 2021, Art. no. 041101, DOI: 10.1063/5.0054128.

[81] H. Wu, W. Fu, Z. Liu, D. Chaw, Y. He, and M. Feng, “Cryo-VCSELs operated at 2.8 K and 40 K with record bandwidth, power and linearity for optical data links in quantum computing,” *IEEE Journal of Quantum Electronics*, vol. 60, no. 5, October 2024, Art. no. 2400310, DOI: 10.1109/JQE.2024.3433450.

[82] B. Namvar, T. Uusitalo, H. Virtanen, M. Guina, and J. Viheriälä, “Improving p-doped DBRs operation at cryogenic temperatures: Investigating different mirror geometry,” *IEEE Photonics Journal*, vol. 16, no. 4, August 2024, Art. no. 1502009, DOI: 10.1109/JPHOT.2024.3402501.

[83] B. Namvar, P. Rajala, M. Guina, T. Hakkarainen, H. Virtanen, T. Uusitalo, and J. Viheriälä, “Thermal characteristics of a double intra-cavity contact VCSEL for cryogenic optical links,” *IEEE Photonics Journal*, vol. 17, no. 5, October 2025, Art. no. 1502406, DOI: 10.1109/JPHOT.2025.3594072.

[84] V. Kaplunenko, M. Khabipov, V. Koshelets, K. Likharev, O. Mukhanov, V. Semenov, I. Serpuchenko, and A. Vystavkin, “Experimental study of the RSFQ logic elements,” *IEEE Transactions on Magnetics*, vol. 25, no. 2, pp. 861–864, March 1989, DOI: 10.1109/20.92422.

[85] “Stony Brook University: Rapid single-flux-quantum laboratory,” Accessed: July 26, 2025, Link.

[86] “SuperTools/ColdFlux RSFQ cell library,” Accessed: July 26, 2025, Link.

[87] S. Li, X. Gao, H. Liu, M. Niu, H. Zhang, X. Zhang, and J. Ren, “CMOS-to-SFQ interface circuits for RZ and NRZ coded signals transformation,” *IEEE Transactions on Applied Superconductivity*, vol. 34, no. 4, June 2024, Art. no. 1400205, DOI: 10.1109/TASC.2024.3376983.

[88] S. K. Tolpygo, V. Bolkhovsky, T. J. Weir, A. Wynn, D. E. Oates, L. M. Johnson, and M. A. Gouker, “Advanced fabrication processes for superconducting very large-scale integrated circuits,” *IEEE Transactions on Applied Superconductivity*, vol. 26, no. 3, April 2016, Art. no. 1100110, DOI: 10.1109/TASC.2016.2519388.

[89] D. Yohannes, M. Renzullo, J. Vivalda, A. Jacobs, M. Yu, J. Walter, A. Kirichenko, I. Vernik, and O. Mukhanov, “High density fabrication process for single flux quantum circuits,” *Applied Physics Letters*, vol. 122, no. 21, May 2023, Art. no. 212601, DOI: 10.1063/5.0152552.

[90] S. Nagasawa, K. Hinode, T. Satoh, M. Hidaka, H. Akaike, A. Fujimaki, N. Yoshikawa, K. Takagi, and N. Takagi, “Nb 9-layer fabrication process for superconducting large-scale SFQ circuits and its process evaluation,” *IEICE Transactions on Electronics*, vol. 97, no. 3, pp. 132–140, March 2014, DOI: 10.1587/transle.E97.C.132.

[91] L. Ying, X. Zhang, M. Niu, J. Ren, W. Peng, M. Maezawa, and Z. Wang, “Development of multi-layer fabrication process for SFQ large scale integrated digital circuits,” *IEEE Transactions on Applied Superconductivity*, vol. 31, no. 5, August 2021, Art. no. 1301504, DOI: 10.1109/TASC.2021.3065277.

[92] J. Kunert, M. Schmelz, K. Peiselt, G. Oelsner, S. Reddy, T. Ortlepp, and R. Stolz, “Advanced FLUXONICS process CJ2 based on sub- μ m-sized cross-type Nb/AlOx/Nb Josephson junctions for mixed signal circuits,” *IEEE Transactions on Applied Superconductivity*, vol. 34, no. 3, May 2024, Art. no. 1101105, DOI: 10.1109/TASC.2024.3355024.

[93] S. Takada, S. Kosaka, and H. Hayakawa, “Current injection logic gate with four Josephson junctions,” *Japanese Journal of Applied Physics*, vol. 19, no. S1, pp. 607–611, 1980, DOI: 10.7567/JJAPS.19S1.607.

[94] H. Nakagawa, E. Sogawa, S. Kosaka, S. Takada, and H. Hayakawa, “Operating characteristics of Josephson four-junction logic (4JL) gate,” *Japanese Journal of Applied Physics*, vol. 21, no. 4A, pp. L198–L200, April 1982, DOI: 10.1143/JJAP.21.L198.

[95] F. China, N. Takeuchi, H. Suzuki, Y. Yamanashi, H. Terai, and N. Yoshikawa, “A high-speed interface based on a Josephson latching driver for adiabatic quantum-flux-parametron logic,” *IEICE Transactions on Electronics*, vol. 105, no. 6, pp. 264–269, June 2022, DOI: 10.1587/transle.2021SEP0002.

[96] Y. Hironaka and N. Yoshikawa, “Josephson latching driver designed using 10 kA/cm² Nb process as interface for Josephson-CMOS hybrid memory,” *IEEE Transactions on Applied Superconductivity*, vol. 35, no. 1, January 2025, Art. no. 1300306, DOI: 10.1109/TASC.2024.3508714.

[97] Y. Hashimoto, S. Yorozu, T. Miyazaki, Y. Kameda, H. Suzuki, and N. Yoshikawa, “Implementation and experimental evaluation of a cryocooled system prototype for high-throughput SFQ digital applications,” *IEEE Transactions on Applied Superconductivity*, vol. 17, no. 2, pp. 546–551, June 2007, DOI: 10.1109/TASC.2007.898126.

[98] A. Hebard, S. Pei, L. Dunkleberger, and T. Fulton, “A dc-powered Josephson flip-flop,” *IEEE Transactions on Magnetics*, vol. 15, no. 1, pp. 408–411, January 1979, DOI: 10.1109/TMAG.1979.1060178.

[99] T. Ortlepp, L. Zheng, S. Whiteley, and T. Van Duzer, “Design guidelines for Suzuki stacks as reliable high-speed Josephson voltage drivers,” *Superconductor Science and Technology*, vol. 26, no. 3, January 2013, Art. no. 035007, DOI: 10.1088/0953-2048/26/3/035007.

[100] T. Ortlepp, S. Wuensch, M. Schubert, P. Febvre, B. Ebert, J. Kunert, E. Crocoll, H.-G. Meyer, M. Siegel, and F. H. Uhlmann, “Superconductor-to-semiconductor interface circuit for high data rates,” *IEEE Transactions on Applied Superconductivity*, vol. 19, no. 1, pp. 28–34, February 2009, DOI: 10.1109/TASC.2008.2009997.

[101] “International Electrotechnical Commission (IEC) 60617 database,” January 2025, Link.

[102] J. A. Delport, K. Jackman, P. Le Roux, and C. J. Fourie, “JoSIM — superconductor SPICE simulator,” *IEEE Transactions on Applied Superconductivity*, vol. 29, no. 5, August 2019, Art. no. 1300905, DOI: 10.1109/TASC.2019.2897312.

[103] Y. Mustafa and S. Köse, “S-PAM: Superconductor-semiconductor interface circuit with pulse-amplitude modulation,” in *IEEE International Symposium on Circuits and Systems (ISCAS)*, May 2025, pp. 1–5, DOI: 10.1109/ISCAS56072.2025.11043921.

[104] V. Kaplunenko, V. Koshelets, M. Khabipov, V. Golomidov, and S. Kovtonyuk, “Single flux quantum quasi-digital voltage amplifier,” *Superconductor Science and Technology*, vol. 4, no. 11, pp. 671–673, 1991, DOI: 10.1088/0953-2048/4/11/032.

[105] K. Krause, Y. Mustafa, A. Shah, S. Köse, and M. C. Hamilton, “Signal integrity simulations of 4JL gate pulses from 4 K to 50 K,” *IEEE Transactions on Applied Superconductivity*, vol. 35, no. 5, August 2025, Art. no. 1300506, DOI: 10.1109/TASC.2024.3510518.

[106] H. Suzuki, A. Inoue, T. Imamura, and S. Hasuo, “A Josephson driver to interface Josephson junctions to semiconductor transistors,” in *IEEE International Electron Devices Meeting*, December 1988, pp. 290–293, DOI: 10.1109/IEDM.1988.32814.

[107] A. Bhat, X. Meng, S. Whiteley, M. Jeffery, and T. Van Duzer, “A 10 GHz digital amplifier in an ultra-small-spread high-J_s/Nb/Al-AlOx/Nb integrated circuit process,” *IEEE Transactions on Applied Superconductivity*, vol. 9, no. 2, pp. 3232–3235, June 1999, DOI: 10.1109/77.783717.

[108] T. Ortlepp, S. R. Whiteley, L. Zheng, X. Meng, and T. Van Duzer, “High-speed hybrid superconductor-to-semiconductor interface circuit with ultra-low power consumption,” *IEEE Transactions on Applied Superconductivity*, vol. 23, no. 3, June 2012, Art. no. 1400104, DOI: 10.1109/TASC.2012.2227918.

[109] N. Harada, A. Yoshida, and N. Yokoyama, “A high-speed Josephson latching driver for a superconducting single-flux-quantum system to semiconductor system interface,” *Japanese Journal of Applied Physics*, vol. 39, no. 11B, p. L1158, November 2000, DOI: 10.1143/JJAP.39.L1158.

[110] T. Hato, M. Horibe, N. Harada, A. Yoshida, Y. Ishimaru, Y. Tarutani, K. Tanabe, and N. Yokoyama, “A high-temperature superconductor latching driver operated at 30 K for a single-flux-

quantum/semiconductor interface," *Superconductor Science and Technology*, vol. 16, no. 12, November 2003, Art. no. 1508, DOI: 10.1088/0953-2048/16/12/041.

[111] H. Suzuki, T. Imamura, and S. Hasuo, "Applications of synchronized switching in series-parallel-connected Josephson junctions," *IEEE Transactions on Electron Devices*, vol. 37, no. 11, pp. 2399–2405, November 1990, DOI: 10.1109/16.62299.

[112] M. Suzuki, M. Maezawa, H. Takato, H. Nakagawa, F. Hirayama, S. Kiryu, M. Aoyagi, T. Sekigawa, and A. Shoji, "An interface circuit for a Josephson-CMOS hybrid digital system," *IEEE Transactions on Applied Superconductivity*, vol. 9, no. 2, pp. 3314–3317, June 1999, DOI: 10.1109/77.783738.

[113] N. Harada, A. Yoshida, and N. Yokoyama, "High-speed demonstration of an output interface driver for single-flux quantum systems," *IEEE Transactions on Applied Superconductivity*, vol. 12, no. 3, pp. 1852–1856, September 2002, DOI: 10.1109/TASC.2002.801814.

[114] J. X. Przybysz, D. Miller, S. Martinet, J. Kang, A. H. Worsham, and M. Farich, "Interface circuits for chip-to-chip data transfer at GHz rates," *IEEE Transactions on Applied Superconductivity*, vol. 7, no. 2, pp. 2657–2660, June 1997, DOI: 10.1109/77.621785.

[115] J. Przybysz, J. McCambridge, P. Dresselhaus, A. Worsham, E. Dean, J. Sage, and T. Weir, "Dewar-to-dewar data transfer at GHz rates," *IEEE Transactions on Applied Superconductivity*, vol. 9, no. 2, pp. 2981–2984, June 1999, DOI: 10.1109/77.783655.

[116] N. Harada, N. Yoshikawa, A. Yoshida, and N. Yokoyama, "Josephson latching driver with a low bit-error rate," *IEEE Transactions on Applied Superconductivity*, vol. 14, no. 4, pp. 2031–2036, December 2004, DOI: 10.1109/TASC.2004.837112.

[117] Y. Feng, X. Meng, S. Whiteley, T. Van Duzer, K. Fujiwara, H. Miyakawa, and N. Yoshikawa, "Josephson-CMOS hybrid memory with ultra-high-speed interface circuit," *IEEE Transactions on Applied Superconductivity*, vol. 13, no. 2, pp. 467–470, June 2003, DOI: 10.1109/TASC.2003.813902.

[118] N. Harada, N. Yoshikawa, K. Yoda, A. Yoshida, and N. Yokoyama, "Logic operation at 5 Gb/s of an output interface for single-flux-quantum systems," *IEEE Transactions on Applied Superconductivity*, vol. 13, no. 3, pp. 3814–3816, September 2003, DOI: 10.1109/TASC.2003.816901.

[119] T. Hato, M. Horibe, H. Wakana, M. Hidaka, and K. Tanabe, "Output interface with latching driver for LTS-SFQ circuits," *IEEE Transactions on Applied Superconductivity*, vol. 15, no. 1, pp. 1–5, March 2005, DOI: 10.1109/TASC.2004.839769.

[120] Y. Mustafa and S. Köse, "Optimization of Suzuki stack circuit to reduce power dissipation," *IEEE Transactions on Applied Superconductivity*, vol. 32, no. 8, November 2022, Art. no. 1301407, DOI: 10.1109/TASC.2022.3192202.

[121] Y. Mustafa and S. Köse, "Suzuki stack circuit with differential output," *IEEE Transactions on Applied Superconductivity*, vol. 33, no. 2, March 2023, Art. no. 1300306, DOI: 10.1109/TASC.2022.3230761.

[122] Q. Liu, T. Van Duzer, X. Meng, S. Whiteley, K. Fujiwara, T. Tomida, K. Tokuda, and N. Yoshikawa, "Simulation and measurements on a 64-kbit hybrid Josephson-CMOS memory," *IEEE Transactions on Applied Superconductivity*, vol. 15, no. 2, pp. 415–418, June 2005, DOI: 10.1109/TASC.2005.849863.

[123] Q. Liu, K. Fujiwara, X. Meng, S. Whiteley, T. Van Duzer, N. Yoshikawa, Y. Thakahashi, T. Hikida, and N. Kawai, "Latency and power measurements on a 64-kb hybrid Josephson-CMOS memory," *IEEE Transactions on Applied Superconductivity*, vol. 17, no. 2, pp. 526–529, June 2007, DOI: 10.1109/TASC.2007.898698.

[124] K. Fujiwara, Q. Liu, T. Van Duzer, X. Meng, and N. Yoshikawa, "New delay-time measurements on a 64-kb Josephson-CMOS hybrid memory with a 600-ps access time," *IEEE Transactions on Applied Superconductivity*, vol. 20, no. 1, pp. 14–20, February 2010, DOI: 10.1109/TASC.2009.2034471.

[125] H. Kojima, Y. Yamashiro, K. Fujiwara, N. Yoshikawa, A. Fujimaki, H. Terai, and S. Yorozi, "Parameter optimization of a Josephson latching driver based on bit-error-rate simulations," *Physica C: Superconductivity and its applications*, vol. 426–431, pp. 1680–1686, October 2005, DOI: 10.1016/j.physc.2005.03.068.

[126] N. Harada, A. Watanabe, Y. Awano, K. Hikosaka, and N. Yokoyama, "A multigigahertz Josephson-semiconductor interface circuit using 77-K differential monolithic HEMT amplifier and 4.2-K JJ high-voltage driver for superconductor-semiconductor electronic hybrid systems," *IEEE Journal of Solid-State Circuits*, vol. 35, no. 1, pp. 66–73, January 2000, DOI: 10.1109/4.818921.

[127] R. D. Sandell, J. W. Spargo, M. Leung, and S. R. Whiteley, "High data rate switch with amplifier chip," *IEEE Transactions on Applied Superconductivity*, vol. 9, no. 2, pp. 2985–2988, June 1999, DOI: 10.1109/77.783656.

[128] T. Van Duzer, Y. Feng, X. Meng, S. R. Whiteley, and N. Yoshikawa, "Hybrid Josephson-CMOS memory: a solution for the Josephson memory problem," *Superconductor Science and Technology*, vol. 15, no. 12, pp. 1669–1674, November 2002, DOI: 10.1088/0953-2048/15/12/307.

[129] H. Suzuki and K. Tanabe, "Superconducting circuit," September 2007, US Patent 7,268,713 B2, Link.

[130] L. Klostermann, S. Trentalange, B. Ritzi, H. Wen, and T. Niinikoski, "Heat sinking of cryogenic coaxial cables in a dilution refrigerator," in *High Energy Spin Physics: Volume 2: Workshops*. Springer, 1991, pp. 378–384, DOI: 10.1007/978-3-642-76661-9_75.

[131] H. Suzuki, M. Maruyama, Y. Hashimoto, K. Fujiwara, and M. Hidaka, "Possible application of flash-type SFQ A/D converter to optical communication systems and their measuring instruments," *IEEE Transactions on Applied Superconductivity*, vol. 19, no. 3, pp. 611–616, June 2009, DOI: 10.1109/TASC.2009.2018034.

[132] Y. Mustafa, K. Krause, A. Shah, M. C. Hamilton, and S. Köse, "DC-biased Suzuki stack circuit for Josephson-CMOS memory applications," *Superconductor Science and Technology*, vol. 37, no. 8, July 2024, Art. no. 085023, DOI: 10.1088/1361-6668/ad5f57.

[133] N. Kotera, A. Asano, Y. Harada, and U. Kawabe, "Ring oscillator experiment using a huffle circuit," *IEEE Transactions on Magnetics*, vol. 19, no. 3, pp. 1174–1177, May 1983, DOI: 10.1109/TMAG.1983.1062274.

[134] Y. Hatano, H. Nagaishi, K. Nakahara, and U. Kawabe, "Performance analysis of the Josephson dc flip-flop," *IEEE Transactions on Applied Superconductivity*, vol. 2, no. 3, pp. 148–155, September 1992, DOI: 10.1109/77.160154.

[135] D. Schneider, J. Lin, S. Polonsky, V. Semenov, and C. Hamilton, "Broadband interfacing of superconducting digital systems to room temperature electronics," *IEEE Transactions on Applied Superconductivity*, vol. 5, no. 2, pp. 3152–3155, June 1995, DOI: 10.1109/77.403260.

[136] S. Polonsky, "New SFQ/DC converter for RSFQ logic/memory family," *Superconductor Science and Technology*, vol. 4, no. 9, pp. 442–444, 1991, DOI: 10.1088/0953-2048/4/9/017.

[137] J. Clarke and A. I. Braginski, *The SQUID handbook: fundamentals and technology of SQUIDs and SQUID systems*. John Wiley & Sons, 2006.

[138] R. P. Welty and J. M. Martinis, "A series array of DC SQUIDS," *IEEE Transactions on Magnetics*, vol. 27, no. 2, pp. 2924–2926, March 1991, DOI: 10.1109/20.133821.

[139] Q. P. Herr, "A high-efficiency superconductor distributed amplifier," *Superconductor Science and Technology*, vol. 23, no. 2, January 2010, Art. no. 022004, DOI: 10.1088/0953-2048/23/2/022004.

[140] R. Koch, P. Ostertag, E. Crocoll, M. Gotz, M. Neuhaus, T. Scherer, M. Winter, and W. Jutzi, "A NRZ-output amplifier for RSFQ circuits," *IEEE Transactions on Applied Superconductivity*, vol. 9, no. 2, pp. 3549–3552, June 1999, DOI: 10.1109/77.783796.

[141] N. B. Dubash, V. V. Borzenets, Y. M. Zhang, V. Kaplunenko, J. W. Spargo, A. Smith, and T. Van Duzer, "System demonstration of a multigigabit network switch," *IEEE Transactions on Microwave Theory and Techniques*, vol. 48, no. 7, pp. 1209–1215, July 2000, DOI: 10.1109/22.853461.

[142] Y. Hashimoto, H. Suzuki, S. Nagasawa, M. Maruyama, K. Fujiwara, and M. Hidaka, "Measurement of superconductive voltage drivers up to 25 Gb/s/ch," *IEEE Transactions on Applied Superconductivity*, vol. 19, no. 3, pp. 1022–1025, June 2009, DOI: 10.1109/TASC.2009.2017867.

[143] H. Terai, S. Miki, and Z. Wang, "Readout electronics using single-flux-quantum circuit technology for superconducting single-photon detector array," *IEEE Transactions on Applied Superconductivity*, vol. 19, no. 3, pp. 350–353, June 2009, DOI: 10.1109/TASC.2009.2019029.

[144] M. Zhao, Y. Wang, X. Gao, P. Yuan, S. Wang, M. Niu, L. You, J. Ren, and L. Li, "A high voltage and high speed superconductive voltage driver using a damped asymmetric DC SQUID array," *Superconductor Science and Technology*, vol. 38, no. 4, March 2025, Art. no. 045011, DOI: 10.1088/1361-6668/adb54.

[145] M. Zhao, Y. Wang, P. Yuan, S. Wang, L. Li, and L. You, "A high-voltage SFQ-to-DC driver for wide-range digital SQUID magnetometer based on flux quanta counting scheme," *Physica C: Superconductivity and its Applications*, vol. 633, June 2025, Art. no. 1354708, DOI: 10.1016/j.physc.2025.1354708.

[146] I. I. Soloviev, M. R. Rafique, H. Engseth, and A. Kidiyarova-Shevchenko, "High voltage driver for RSFQ digital signal processor," *IEEE Transactions on Applied Superconductivity*, vol. 17, no. 2, pp. 470–473, June 2007, DOI: 10.1109/TASC.2007.898070.

[147] M. Khabipov, D. Hagedorn, F.-I. Buchholz, J. Kohlmann, F. Maibaum, M. Schilling, and J. Niemeyer, "Development of RSFQ voltage drivers for arbitrary AC waveform synthesizers," in *Journal of Physics: Conference Series*, vol. 43, no. 1. IOP Publishing, 2006, pp. 1175–1178, DOI: 10.1088/1742-6596/43/1/286.

[148] S. Razmkhah, A. Bozbey, and P. Febvre, "A compact high frequency voltage amplifier for superconductor–semiconductor logic interface," *Superconductor Science and Technology*, vol. 34, no. 4, February 2021, Art. no. 045013, DOI: 10.1088/1361-6668/abdedb.

[149] O. Mukhanov, S. V. Rylov, D. V. Gaidarenko, N. B. Dubash, and V. V. Borzenets, "Josephson output interfaces for RSFQ circuits," *IEEE Transactions on Applied Superconductivity*, vol. 7, no. 2, pp. 2826–2831, June 1997, DOI: 10.1109/77.621825.

[150] N. Yoshikawa, T. Abe, Y. Kato, and H. Hoshina, "Component development for a 16 Gb/s RSFQ–CMOS interface system," *IEEE Transactions on Applied Superconductivity*, vol. 11, no. 1, pp. 735–738, March 2001, DOI: 10.1109/77.919450.

[151] A. Inamdar, S. Rylov, S. Sarwana, and D. Gupta, "Superconducting switching amplifiers for high speed digital data links," *IEEE Transactions on Applied Superconductivity*, vol. 19, no. 3, pp. 1026–1033, June 2009, DOI: 10.1109/TASC.2009.2018413.

[152] Y. Tarutani, K. Saitoh, and K. Takagi, "Interface circuit using JTLs as control lines of SQUID array," *IEEE Transactions on Applied Superconductivity*, vol. 11, no. 1, pp. 341–344, March 2001, DOI: 10.1109/77.919352.

[153] F. Hirayama, M. Maezawa, S. Kiryu, H. Sasaki, and A. Shoji, "Characteristics of a voltage multiplier for a RSFQ digital-to-analog converter," *Superconductor Science and Technology*, vol. 15, no. 4, pp. 494–498, February 2002, DOI: 10.1088/0953-2048/15/4/303.

[154] F. Aghighi, S. Jamasb, and M. Mazaheri, "Level shifting circuit for hybrid superconductor-to-semiconductor interface," *Physica C: Superconductivity and its Applications*, vol. 552, pp. 57–60, September 2018, DOI: 10.1016/j.physc.2018.05.017.

[155] D. Wei, S. R. Whiteley, L. Zheng, H. Park, H. Kim, and T. Van Duzer, "New Josephson–CMOS interface amplifier," *IEEE Transactions on Applied Superconductivity*, vol. 21, no. 3, pp. 805–808, June 2010, DOI: 10.1109/TASC.2010.2088358.

[156] J. Egan, A. Brownfield, and Q. Herr, "True differential superconducting on-chip output amplifier," *Superconductor Science and Technology*, vol. 35, no. 4, March 2022, Art. no. 045018, DOI: 10.1088/1361-6668/ac5314.

[157] Q. P. Herr, D. L. Miller, A. A. Pesetski, and J. X. Przybysz, "Inductive isolation in stacked SQUID amplifiers," *IEEE Transactions on Applied Superconductivity*, vol. 17, no. 2, pp. 565–568, June 2007, DOI: 10.1109/TASC.2007.898542.

[158] T. M. T. Morooka, "Design, fabrication and evaluation of a four-josephson-junction superconducting quantum interference device with two superconducting loops," *Japanese Journal of Applied Physics*, vol. 36, no. 12A, pp. L1587–L1590, December 1997, DOI: 10.1143/JJAP.36.L1587.

[159] K. Higuchi, H. Shimada, and Y. Mizugaki, "Design and operation of distributed double-SQUID amplifier for RSFQ circuits," in *Journal of Physics: Conference Series*, vol. 1293, no. 1. IOP Publishing, 2019, Art. no. 012060, DOI: 10.1088/1742-6596/1293/1/012060.

[160] Y. Mizugaki, K. Higuchi, and H. Shimada, "Enhanced voltage swing of rapid-single-flux-quantum distributed output amplifier equipped with double-stack superconducting quantum interference devices," *IEICE Electronics Express*, vol. 16, no. 14, pp. 1–4, August 2019, DOI: 10.1587/elex.16.20190331.

[161] V. K. Kornev, I. I. Soloviev, N. V. Klenov, and O. A. Mukhanov, "Development of SQIF-based output broad band amplifier," *IEEE Transactions on Applied Superconductivity*, vol. 17, no. 2, pp. 569–572, June 2007, DOI: 10.1109/TASC.2007.898119.

[162] M. A. Castellanos-Beltran, D. Olaya, A. Sirois, C. Donnelly, P. Dresselhaus, S. Benz, and P. Hopkins, "Single-flux-quantum multiplier circuits for synthesizing gigahertz waveforms with quantum-based accuracy," *IEEE Transactions on Applied Superconductivity*, vol. 31, no. 3, April 2021, Art. no. 1400109, DOI: 10.1109/TASC.2021.3057013.

[163] F. Hirayama, M. Maezawa, H. Sasaki, and A. Shoji, "Characteristics of voltage multipliers for a Josephson D/A converter," *IEEE Transactions on Applied Superconductivity*, vol. 13, no. 2, pp. 484–487, June 2003, DOI: 10.1109/TASC.2003.813912.

[164] M. Tanaka, Y. Kitagawa, T. Satoh, and T. Yamamoto, "Low-power single-flux-quantum standard cell library using 250 A/cm² process for qubit control applications," *IEEE Transactions on Applied Superconductivity*, vol. 35, no. 5, August 2025, Art. no. 1700405, DOI: 10.1109/TASC.2024.3521892.

[165] M. Maezawa, F. Hirayama, and M. Suzuki, "Design and fabrication of RSFQ cell library for middle-scale applications," *Physica C: Superconductivity*, vol. 412–414, pp. 1591–1596, October 2004, DOI: 10.1016/j.physc.2004.02.221.

[166] H. Cong, S. Razmkhah, M. A. Karamuftuoglu, and M. Pedram, "Superconductor logic implementation with all-JJ inductor-free cell library," *IEEE Transactions on Applied Superconductivity*, vol. 34, no. 9, December 2024, Art. no. 1301110, DOI: 10.1109/TASC.2024.3430975.

[167] Z. Chen, L. Li, and L. You, "Signal matching from SFQ/DC converter to SiGe BiCMOS interface," *IEICE Electronics Express*, vol. 21, no. 1, pp. 1–6, May 2025, DOI: 10.1587/elex.22.20250196.

[168] S. Wuensch, T. Ortlepp, E. Crocoll, F. H. Uhlmann, and M. Siegel, "Cryogenic semiconductor amplifier for RSFQ-circuits with high data rates at 4.2 K," *IEEE Transactions on Applied Superconductivity*, vol. 19, no. 3, pp. 574–579, June 2009, DOI: 10.1109/TASC.2009.2018425.

[169] V. Golomidov, V. Kaplunenko, M. Khabipov, V. Koshelets, and O. Kaplunenko, "Single flux quantum voltage amplifiers," *Cryogenics*, vol. 32, pp. 509–512, 1992, DOI: 10.1016/0011-2275(92)90217-X.

[170] Q. P. Herr, "Stacked double-flux-quantum output amplifier," *IEEE Transactions on Applied Superconductivity*, vol. 15, no. 2, pp. 259–262, June 2005, DOI: 10.1109/TASC.2005.849784.

[171] Y. Somei, H. Shimada, and Y. Mizugaki, "Enhanced operation frequencies of bipolar double-flux-quantum amplifiers fabricated using 10 kA cm⁻² Nb/AlOx/Nb integration process," *Japanese Journal of Applied Physics*, vol. 60, no. 7, July 2021, Art. no. 073001, DOI: 10.35848/1347-4065/ac0450.

[172] Y. Mizugaki, Y. Arai, T. Watanabe, and H. Shimada, "1000-fold double-flux-quantum voltage multiplier employing directional propagation of flux quanta through asymmetrically damped junction branches," *IEEE Transactions on Applied Superconductivity*, vol. 29, no. 5, August 2019, Art. no. 1400105, DOI: 10.1109/TASC.2019.2895606.

[173] D. A. Buck, "The cryotron-a superconductive computer component," *Proceedings of the IRE*, vol. 44, no. 4, pp. 482–493, April 1956, DOI: 10.1109/JRPROC.1956.274927.

[174] A. N. McCaughan and K. K. Berggren, "A superconducting-nanowire three-terminal electrothermal device," *Nano letters*, vol. 14, no. 10, pp. 5748–5753, September 2014, DOI: 10.1021/nl502629x.

[175] Q.-Y. Zhao, A. N. McCaughan, A. E. Dane, K. K. Berggren, and T. Ortlepp, "A nanocryotron comparator can connect single-flux-quantum circuits to conventional electronics," *Superconductor Science and Technology*, vol. 30, no. 4, March 2017, Art. no. 044002, DOI: 10.1088/1361-6668/aa5f33.

[176] M. Tanaka, M. Suzuki, G. Konno, Y. Ito, A. Fujimaki, and N. Yoshikawa, "Josephson–CMOS hybrid memory with nanocryotrons," *IEEE Transactions on Applied Superconductivity*, vol. 27, no. 4, June 2017, Art. no. 1800904, DOI: 10.1109/TASC.2016.2646929.

[177] K. Sano, M. Suzuki, K. Maruyama, S. Taniguchi, M. Tanaka, A. Fujimaki, M. Inoue, and N. Yoshikawa, "Thermally assisted superconductor transistors for Josephson–CMOS hybrid memories," *IEICE Transactions on Electronics*, vol. 101, no. 5, pp. 370–377, May 2018, DOI: 10.1587/transle.E101.C.370.

[178] R. Baghdadi, J. P. Allmaras, B. A. Butters, A. E. Dane, S. Iqbal, A. N. McCaughan, E. A. Toomey, Q.-Y. Zhao, A. G. Kozorezov, and K. K. Berggren, "Multilayered heater nanocryotron: A superconducting-nanowire-based thermal switch," *Physical Review Applied*, vol. 14, no. 5, November 2020, Art. no. 054011, DOI: 10.1103/PhysRevApplied.14.054011.

[179] A. N. McCaughan, V. B. Verma, S. M. Buckley, J. Allmaras, A. Kozorezov, A. Tait, S. Nam, and J. Shainline, "A superconducting thermal switch with ultrahigh impedance for interfacing superconductors to semiconductors," *Nature Electronics*, vol. 2, no. 10, pp. 451–456, September 2019, DOI: 10.1038/s41928-019-0300-8.

[180] D. J. Paul, T. X. Zhou, and K. K. Berggren, "Photolithography-compatible three-terminal superconducting switch for driving CMOS loads," *Physical Review Applied*, vol. 24, no. 2, August 2025, Art. no. 024060, DOI: 10.1103/261b-37xx.

[181] N. Yasukawa, T. Nishio, and Y. Mawatari, "Ginzburg–Landau simulations of three-terminal operation of a superconducting nanowire cryotron," *Superconductor Science and Technology*, vol. 37, no. 6, May 2024, Art. no. 065013, DOI: 10.1088/1361-6668/ad44e4.

[182] Q.-Y. Zhao, E. A. Toomey, B. A. Butters, A. N. McCaughan, A. E. Dane, S.-W. Nam, and K. K. Berggren, "A compact superconducting nanowire memory element operated by nanowire cryotrons," *Superconductor Science and Technology*, vol. 31, no. 3, February 2018, Art. no. 035009, DOI: 10.1088/1361-6668/aaa820.

[183] M.-H. Nguyen, G. J. Ribeill, M. V. Gustafsson, S. Shi, S. V. Aradhya, A. P. Wagner, L. M. Ranzani, L. Zhu, R. Baghdadi, B. Butters *et al.*, "Cryogenic memory architecture integrating spin Hall effect based magnetic memory and superconductive cryotron devices," *Scientific Reports*, vol. 10, no. 1, January 2020, Art. no. 248, DOI: 10.1038/s41598-019-57137-9.

[184] S. Alam, D. S. Rampini, B. G. Oripov, A. N. McCaughan, and A. Aziz, "Cryogenic reconfigurable logic with superconducting heater cryotron: Enhancing area efficiency and enabling camouflaged processors," *Applied Physics Letters*, vol. 123, no. 15, October 2023, Art. no. 152603, DOI: 10.1063/5.0170187.

[185] V. Karam, O. Medeiros, T. E. Dandachi, M. Castellani, R. Foster, K. Berggren, and M. Colangelo, "Parameter extraction for a SPICE model of an hTron superconducting thermal switch," *Physical Review Applied*, vol. 24, no. 2, August 2025, Art. no. 024020, DOI: 10.1103/jdzc-712x.

[186] J. M. Shainline, S. M. Buckley, A. N. McCaughan, J. Chiles, A. Jafari-Salim, R. P. Mirin, and S. W. Nam, "Circuit designs for superconducting optoelectronic loop neurons," *Journal of Applied Physics*, vol. 124, no. 15, October 2018, Art. no. 152130, DOI: 10.1063/1.5038031.

[187] S. Faris, S. Raider, W. Gallagher, and R. Drake, "Quiteron," *IEEE Transactions on Magnetics*, vol. 19, no. 3, pp. 1293–1295, May 2003, DOI: 10.1109/TMAG.1983.1062499.

[188] D. J. Frank, "A circuit-oriented quiteron analysis," *Journal of Applied Physics*, vol. 56, no. 9, pp. 2553–2557, May 1984, DOI: 10.1063/1.334320.

[189] T. Nishino, M. Hatano, H. Hasegawa, F. Murai, T. Kure, A. Hiraiwa, K. Yagi, and U. Kawabe, "0.1- μ m gate-length superconducting FET," *IEEE Electron Device Letters*, vol. 10, no. 2, pp. 61–63, February 1989, DOI: 10.1109/55.32429.

[190] I. Nevirkovets, "A superconducting transistorlike device having good input-output isolation," *Applied Physics Letters*, vol. 95, no. 5, August 2009, Art. no. 052505, DOI: 10.1063/1.3189283.

[191] I. P. Nevirkovets, O. Chernyashevskyy, G. V. Prokopenko, O. A. Mukhanov, and J. B. Ketterson, "Superconducting-ferromagnetic transistor," *IEEE Transactions on Applied Superconductivity*, vol. 24, no. 4, August 2014, Art. no. 1800506, DOI: 10.1109/TASC.2014.2318317.

[192] I. P. Nevirkovets, T. Kojima, Y. Uzawa, P. G. Kotula, N. Missett, and O. A. Mukhanov, "Characterization of amplification properties of the superconducting-ferromagnetic transistor," *IEEE Transactions on Applied Superconductivity*, vol. 30, no. 7, October 2020, Art. no. 1800105, DOI: 10.1109/TASC.2020.2992992.

[193] I. Nevirkovets and O. Mukhanov, "Electrically controlled hybrid superconductor-ferromagnet cell for high density cryogenic memory," *Applied Physics Letters*, vol. 123, no. 7, August 2023, Art. no. 072601, DOI: 10.1063/5.0165128.

[194] T. Akazaki, H. Takayanagi, J. Nitta, and T. Enoki, "A Josephson field effect transistor using an inas-inserted-channel $In_{0.52}Al_{0.48}As/In_{0.53}Ga_{0.47}As$ inverted modulation-doped structure," *Applied Physics Letters*, vol. 68, no. 3, pp. 418–420, January 1996, DOI: 10.1063/1.116704.

[195] G. De Simoni, F. Paolucci, C. Puglia, and F. Giazotto, "Josephson field-effect transistors based on all-metallic Al/Cu/Al proximity nanojunctions," *ACS nano*, vol. 13, no. 7, pp. 7871–7876, June 2019, DOI: 10.1021/acsnano.9b02209.

[196] F. Wen, J. Shabani, and E. Tutuc, "Josephson junction field-effect transistors for boolean logic cryogenic applications," *IEEE Transactions on Electron Devices*, vol. 66, no. 12, pp. 5367–5374, December 2019, DOI: 10.1109/TED.2019.2951634.

[197] F. Paolucci, G. De Simoni, E. Strambini, P. Solinas, and F. Giazotto, "Ultra-efficient superconducting Dayem bridge field-effect transistor," *Nano Letters*, vol. 18, no. 7, pp. 4195–4199, June 2018, DOI: 10.1021/acs.nanolett.8b01010.

[198] G. De Simoni, F. Paolucci, P. Solinas, E. Strambini, and F. Giazotto, "Metallic supercurrent field-effect transistor," *Nature Nanotechnology*, vol. 13, no. 9, pp. 802–805, September 2018, DOI: 10.1038/s41565-018-0190-3.

[199] F. Giazotto, J. T. Peltonen, M. Meschke, and J. P. Pekola, "Superconducting quantum interference proximity transistor," *Nature Physics*, vol. 6, no. 4, pp. 254–259, April 2010, DOI: 10.1038/nphys1537.

[200] D. Gupta, J. C. Bardin, A. Inamdar, A. Dayalu, S. Sarwana, P. Ravindran, S.-W. Chang, A. H. Coskun, and M. G. Sadrabadi, "Low-power high-speed hybrid temperature heterogeneous technology digital data link," *IEEE Transactions on Applied Superconductivity*, vol. 23, no. 3, June 2013, Art. no. 1701806, DOI: 10.1109/TASC.2013.2257231.

[201] P. Ravindran, S.-W. Chang, D. Gupta, A. Inamdar, V. Dotsenko, S. M. Sarwana, and J. C. Bardin, "Power-optimized temperature-distributed digital data link," *IEEE Transactions on Applied Superconductivity*, vol. 25, no. 3, June 2014, Art. no. 1300605, DOI: 10.1109/TASC.2014.2372339.

[202] P. Ravindran, S.-W. Chang, W.-T. Wong, S. M. Sarwana, V. Dotsenko, J. Tang, S. Ruotolo, D. Gupta, and J. C. Bardin, "Energy efficient digital data link," *IEEE Transactions on Applied Superconductivity*, vol. 27, no. 4, June 2017, Art. no. 1301105, DOI: 10.1109/TASC.2016.2636252.

[203] Z. Chen, X. Zhang, L. You, and L. Li, "A SFQ-to-CMOS interface circuit based on SiGe BiCMOS for Josephson-CMOS hybrid system," *Journal of Low Temperature Physics*, vol. 219, pp. 196–208, April 2025, DOI: 10.1007/s10909-025-03291-6.

[204] I. Soloviev, V. Ruzhickiy, S. Bakurskiy, N. Klenov, M. Y. Kupriyanov, A. Golubov, O. Skryabina, and V. Stolyarov, "Superconducting circuits without inductors based on bistable Josephson junctions," *Physical Review Applied*, vol. 16, no. 1, July 2021, Art. no. 014052, DOI: 10.1103/PhysRevApplied.16.014052.

[205] T. Jabbari, M. Bocko, and E. G. Friedman, "All-JJ logic based on bistable JJs," *IEEE Transactions on Applied Superconductivity*, vol. 33, no. 5, August 2023, Art. no. 1303807, DOI: 10.1109/TASC.2023.3260774.

[206] E. Elmitewalli and S. Köse, "Bistable Josephson junction-based true random number generator without inductors," *IEEE Transactions on Circuits and Systems II: Express Briefs*, vol. 70, no. 4, pp. 1615–1619, April 2023, DOI: 10.1109/TCSII.2022.3226166.

[207] I. Salameh, E. G. Friedman, and S. Kvatin斯基, "Superconductive logic using 2ϕ -Josephson junctions with half flux quantum pulses," *IEEE Transactions on Circuits and Systems II: Express Briefs*, vol. 69, no. 5, pp. 2533–2537, May 2022, DOI: 10.1109/TCSII.2022.3162723.

[208] A. Mitrovic and M. Bocko, "Josephson junctions with ferromagnetic barriers for digital superconducting electronics: A review," *Physical Review Applied*, vol. 23, no. 6, June 2025, Art. no. 067001, DOI: 10.1103/PhysRevApplied.23.067001.

[209] Q. Liu, "Josephson-CMOS hybrid memories," Ph.D. dissertation, University of California, Berkeley, 2007.

[210] T. Hato, Y. Ishimaru, N. Harada, M. Horibe, A. Yoshida, Y. Tarutani, K. Tanabe, and N. Yokoyama, "SFQ-to-level logic conversion by HTS Josephson drivers for output interface," *IEEE Transactions on Applied Superconductivity*, vol. 13, no. 2, pp. 397–400, June 2003, DOI: 10.1109/TASC.2003.813867.

[211] H. Jin, K. Kuwabara, Y. Yamanashi, and N. Yoshikawa, "Investigation of robust CMOS amplifiers for Josephson-CMOS hybrid memories," *Physics Procedia*, vol. 36, pp. 229–234, September 2012, DOI: 10.1016/j.phpro.2012.06.151.

[212] K. Kuwabara, H. Jin, Y. Yamanashi, and N. Yoshikawa, "Design and implementation of 64-kb CMOS static RAMs for Josephson-CMOS hybrid memories," *IEEE Transactions on Applied Superconductivity*, vol. 23, no. 3, June 2013, Art. no. 1700704, DOI: 10.1109/TASC.2012.2229331.

[213] E. Salman and E. G. Friedman, *High performance integrated circuit design*. McGraw Hill Professional, 2012.

[214] U. Ghoshal, H. Kroger, and T. Van Duzer, "Superconductor-semiconductor memories," *IEEE Transactions on Applied Superconductivity*, vol. 3, no. 1, pp. 2315–2318, March 1993, DOI: 10.1109/77.233542.

[215] U. Ghoshal, S. Kishore, A. Feldman, L. Huynh, and T. Van Duzer, "CMOS amplifier designs for Josephson-CMOS interface circuits," *IEEE Transactions on Applied Superconductivity*, vol. 5, no. 2, pp. 2640–2643, June 1995, DOI: 10.1109/77.403132.

[216] S. Krinner, S. Storz, P. Kurpiers, P. Magnard, J. Heinsoo, R. Keller, J. Luetolf, C. Eichler, and A. Wallraff, "Engineering cryogenic setups for 100-qubit scale superconducting circuit systems," *EPJ Quantum Technology*, vol. 6, no. 2, pp. 1–29, May 2019, DOI: 10.1140/epjqt/s40507-019-0072-0.

[217] N. Zhudassov and E. G. Friedman, *Cryogenic Microelectronic Systems for Ultra-Low Energy and Enhanced Performance*. Springer Nature, 2025.

[218] Y. Mustafa and S. Köse, "Ternary digital output data link from SFQ circuits," *IEEE Transactions on Applied Superconductivity*, vol. 35, no. 5, August 2025, Art. no. 1300405, DOI: 10.1109/TASC.2024.3510520.

[219] R. Robertazzi, I. Siddiqi, and O. Mukhanov, "Flux trapping experiments in single flux quantum shift registers," *IEEE Transactions on Applied Superconductivity*, vol. 7, no. 2, pp. 3164–3167, June 1997, DOI: 10.1109/77.622002.

[220] C. J. Fourie and K. Jackman, "Experimental verification of moat design and flux trapping analysis," *IEEE Transactions on Applied*

Superconductivity, vol. 31, no. 5, August 2021, Art. no. 1300507, DOI: 10.1109/TASC.2021.3051582.

[221] X. Peng, X. Liu, Y. Mei, J. Ren, and H. Tang, “A solution for ultra-low bit-error-rate interface of superconductor-semiconductor by using an error-correction-code encoder,” *IEEE Transactions on Applied Superconductivity*, vol. 29, no. 5, August 2019, Art. no. 1301604, DOI: 10.1109/TASC.2019.2900581.

[222] Y. Mustafa, B. Peköz, and S. Köse, “Lightweight error-correction code encoders in superconducting electronic systems,” *arXiv preprint arXiv:2509.00962*, 2025, DOI: 10.48550/arXiv.2509.00962.

[223] Y. Mustafa and S. Köse, “Side-channel leakage in SFQ circuits and related attacks on qubit control and readout systems,” *IEEE Transactions on Applied Superconductivity*, vol. 33, no. 6, September 2023, Art. no. 1304307, DOI: 10.1109/TASC.2023.3277864.

[224] Y. Mustafa and S. Köse, “Side-channel leakage in Suzuki stack circuits,” in *Quantum Computing: Circuits, Systems, Automation and Applications*. Springer, 2024, pp. 55–67, DOI: 10.1007/978-3-031-37966-6_3.

[225] Y. Mustafa and S. Köse, “Side-channel attacks targeting classical-quantum interface in quantum computers,” in *IEEE International Symposium on Circuits and Systems (ISCAS)*. IEEE, May 2024, pp. 1–5, DOI: 10.1109/ISCAS58744.2024.10558006.

[226] Y. Mustafa and S. Köse, “Built-in self-test of SFQ circuits using side-channel leakage information,” *IEEE Transactions on Very Large Scale Integration (VLSI) Systems*, vol. 32, no. 6, pp. 1100–1109, June 2024, DOI: 10.1109/TVLSI.2024.3385014.